Epigenetic Metabolic Reprogramming of Right Ventricular Fibroblasts in Pulmonary Arterial Hypertension: A Pyruvate Dehydrogenase Kinase-Dependent Shift in Mitochondrial Metabolism Promotes Right Ventricular Fibrosis

Lian Tian[1], **Danchen Wu**[1], **Asish Dasgupta**[1], **Kuang-Hueih Chen**[1], **Jeffrey Mewburn**[1], **Francois Potus**[1], **Patricia A.D. Lima**[2], **Zhigang Hong**[3], **Yuan-Yuan Zhao**[4], **Charles C.T. Hindmarch**[2], **Shelby Kutty**[5], **Steeve Provencher**[6], **Sebastien Bonnet**[6], **Gopinath Sutendra**[7], **Stephen L. Archer**[1,2]

[1]Medicine, Queen's University, Kingston, Ontario, Canada

[2]Queen's Cardiopulmonary Unit (QCPU), Translational Institute of Medicine (TIME), Department of Medicine, Queen's University, Kingston, Ontario, Canada

[3]Pharmacology, University of Illinois at Chicago, Chicago, Illinois, USA

[4]Agricultural, Food and Nutritional Science, University of Alberta, Edmonton, Alberta, Canada

[5]Medicine, John Hopkins University, Baltimore, Maryland, USA

[6]Pulmonary Hypertension Research Group, Heart and Lung Institute of Quebec, Department of Medicine, Laval University, Quebec City, Quebec, Canada

[7]Medicine, University of Alberta, Edmonton, Alberta, Canada.

Abstract

Rationale—Right ventricular (RV) fibrosis in pulmonary arterial hypertension (PAH) contributes to RV failure (RVF). While RV fibrosis reflects changes in the function of resident RV fibroblasts (RVfib), these cells are understudied.

Objective—Examine the role of mitochondrial metabolism of RVfib in RV fibrosis in human and experimental PAH.

Methods and Results—Male Sprague-Dawley rats received monocrotaline (MCT; 60 mg/kg) or saline. Drinking water containing no supplement or the pyruvate dehydrogenase kinase (PDK) inhibitor dichloroacetate was started 7-days post MCT. At week-4, treadmill testing, echocardiography and right heart catheterization were performed. The effects of PDK activation on mitochondrial dynamics and metabolism, RVfib proliferation, and collagen production were studied in RVfib in cell culture. Epigenetic mechanisms for persistence of the profibrotic RVfib

Address correspondence to: Dr. Stephen L. Archer, Tier 1 CRC Mitochondrial Dynamics, Elizabeth Smith Distinguished Professor, Head Department of Medicine, Queen's University, Director Queen's Cardiopulmonary Unit, Program Medical Director for Medicine and Cardiac Sciences at KGH, HDH, SMOL, Etherington Hall, Room 3041, 94 Stuart St., Kingston, Ontario, Canada, K7L 3N6, stephen.archer@queensu.ca.
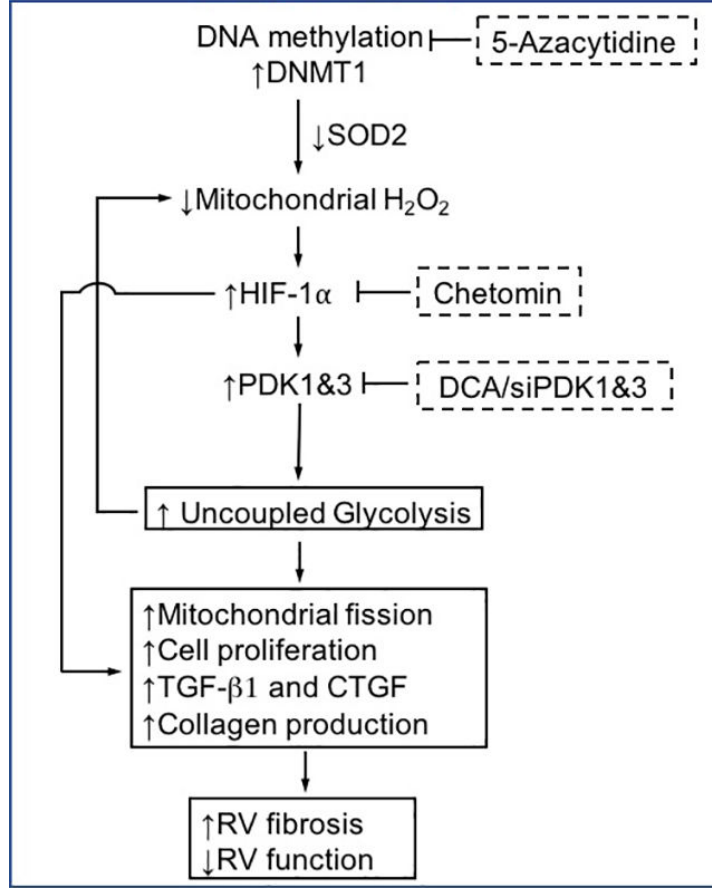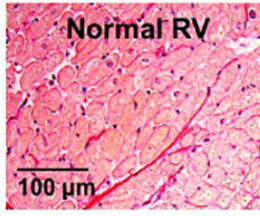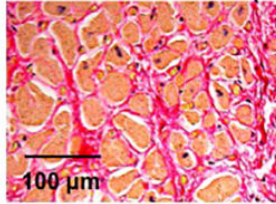
phenotype in culture were evaluated. PDK expression was also studied in the RVfib of patients with decompensated RVF (n=11) versus control (n=7). MCT rats developed PAH, RV fibrosis and RVF. MCT-RVfib (but not left ventricular fibroblasts) displayed excess mitochondrial fission and had increased expression of PDK isoforms 1&3 that persisted for >5 passages in culture. PDK-mediated decreases in pyruvate dehydrogenase (PDH) activity and oxygen-consumption rate were reversed by dichloroacetate (in RVfib and *in vivo*) or siRNA targeting PDK 1&3 (in RVfib). These interventions restored mitochondrial superoxide and H_2O_2 production and inactivated hypoxia-inducible factor 1-alpha (HIF-1α), which was pathologically activated in normoxic MCT-RVfib. Redox-mediated HIF-1α inactivation also decreased expression of transforming growth factor beta-1 and connective tissue growth factor, reduced fibroblast proliferation, and decreased collagen production. HIF-1α activation in MCT-RVfib reflected increased DNA methyltransferase 1 (DNMT1) expression, which was associated with a decrease in its regulatory microRNA, miR-148b-3p. In MCT rats, dichloroacetate, at therapeutic levels in the RV, reduced phospho-PDH expression, RV fibrosis and hypertrophy, and improved RV function. In patients with PAH and RVF, RVfib had increased PDK1 expression.

Conclusions—MCT-RVfib manifest a DNMT1-HIF-1α-PDK-mediated, chamber-specific, metabolic memory that promotes collagen production and RV fibrosis. This epigenetic mitochondrial-metabolic pathway is a potential antifibrotic therapeutic target.

Graphical Abstract

Normal RV

100 μm

DNA methylation ⊢── 5-Azacytidine
↑DNMT1

↓SOD2

↓Mitochondrial H₂O₂

↑HIF-1α ⊢── Chetomin

↑PDK1&3 ⊢── DCA/siPDK1&3

↑ Uncoupled Glycolysis

↑Mitochondrial fission
↑Cell proliferation
↑TGF-β1 and CTGF
↑Collagen production

↑RV fibrosis
↓RV function

PAH: Fibrotic RV (red)

100 μm

INTRODUCTION

In pulmonary arterial hypertension (PAH), prognosis is substantially determined by the response of the right ventricle (RV) to increases in pulmonary vascular resistance (PVR) and mean pulmonary artery pressure (mPAP).[1–7] Some patients with PAH are adaptive remodelers and retain RV function despite increased afterload; whereas others are maladaptive remodelers and rapidly develop RV failure (RVF).[8] The failing RV is characterized by dilatation and fibrosis, resulting from autonomic nervous system activation, [9] ischemia (due to impaired epicardial coronary artery perfusion pressure[10], microvascular ischemia[11] and/or capillary rarefaction,[12–14]) and mitochondrial metabolic abnormalities, including a shift to uncoupled aerobic glycolysis,[15, 16] reviewed in.[8] RV fibrosis is a ubiquitous, but under-studied feature of maladaptive RV hypertrophy (RVH). RV fibrosis, which occurs in maladaptive RVH in PAH patients[17] and rodent models of PAH,[12, 18–20] reduces RV compliance and predicts poor outcome.[21, 22] RV pressure overload activates RV fibroblasts (RVfib), which produce more extracellular matrix, in part because of activation of genes that regulate collagen production, such as transforming growth factor beta-1 (TGF-β1) and connective tissue growth factor (CTGF).[20, 23] While appropriate collagen deposition is necessary for maintaining RV structure, excessive fibrosis may increase RV stiffness and contribute to RVF. The mechanisms underlying RVfib activation and collagen production are under studied.

In PAH, pulmonary artery (PA) smooth muscle cells (PASMC),[24] PA adventitial fibroblasts (PAfib),[25–27] PA endothelial cells (PAEC)[28, 29] and RV cardiomyocytes[30–32] develop a metabolic shift characterized by reduced glucose oxidation and increased uncoupled glycolysis, referred to as the Warburg effect. These acquired mitochondrial metabolic abnormalities contribute to disease pathology, promoting hyperproliferation and apoptosis resistance in PASMC, PAfib and PAEC while inducing hypocontractility in RV cardiomyocytes. In PASMC, PAfib and RV cardiomyocytes in PAH, the metabolic shift is driven by activation of pyruvate dehydrogenase kinase (PDK), a family of 4 enzyme isoforms that phosphorylates and inhibits pyruvate dehydrogenase (PDH), a key enzyme in mitochondrial glucose oxidation.[27, 30, 33–36] The upregulation of PDK in PAH partially reflects abnormal activation of hypoxia inducible factor (HIF-1α), an established transcriptional regulator of PDK.[37] HIF-1α activation in PAH occurs, at least in part from epigenetic silencing of mitochondrial redox signaling, notably a depression of mitochondrial derived hydrogen peroxide production by superoxide dismutase 2 (SOD2).[38] Glucose uptake via the glucose transporter (Glut) is enhanced in both RV and lung from monocrotaline (MCT) and Sugen-Hypoxia rats and PAH patients.[15, 16, 24, 30, 31, 36, 39] This compensatory increase in glucose flux is required to support energy homeostasis in the presence of uncoupled glycolysis, which yields only ~$1/16^{th}$ the ATP/mol of glucose that results from coupled glycolysis and glucose oxidation. A PDK inhibitor, sodium dichloroacetate (DCA), restores mitochondrial glucose metabolism and inhibits cell proliferation and apoptosis resistance in PASMC[35, 40] and PAfib[27, 36] and enhances RV contractility *ex vivo*.[30] DCA improves RV function and oxidative glucose metabolism *in vivo* in preclinical models of PAH[33] and in some patients with idiopathic PAH.[34]

The Warburg metabolic shift can also be mediated by an additional epigenetic mechanism, the alteration of the expression and function of splice variants of pyruvate kinase (PK), the terminal enzyme in the glycolytic cascade. Decreased expression of microRNA (miR)-124 expression in PAfib[25] and PAEC[28] in PAH increases polypyrimidine tract-binding protein 1 (PTBP1) expression. PTBP1 alters PK splicing, increasing the ratio of PK muscle isoform 2 to isoform 1 (PKM2/PKM1), which favors uncoupled glycolysis. This mechanism is associated with a decreased expression of the mitochondrial pyruvate carrier (MPC), further depriving mitochondria of substrate for Krebs cycle.[25, 28] It is unknown whether PDK activation and/or a PKM2/PKM1 isoform switch contribute to the hyperproliferative, fibrogenic phenotype of RVfib in PAH.

Using the MCT rat model of PAH, we isolated MCT-RVfib and left ventricular (LV) fibroblasts (LVfib). RVfib (but not LVfib) were epigenetically reprogrammed to a hyperproliferative, fibrogenic phenotype that persisted in cell culture for multiple passages. This phenotype occurred by a PDK-dependent mechanism, without changes in PKM or MPC. PDK inhibition, using DCA or small interfering RNA targeting the upregulated PDK isoforms 1 and 3 (siPDK1&3), improved glucose oxidation and reduced proliferation rate and collagen production in MCT-RVfib. Patients with PAH and RVF also had increased expression of PDK1 in their RVfib. We identified an epigenetic mechanism for PDK activation in MCT-RVfib. Upregulation of DNA methyltransferase 1 (DNMT1) depresses SOD2 expression, reduces mitochondrial hydrogen peroxide (H_2O_2) production, and triggers normoxic HIF-1α activation in MCT-RVfib. HIF-1α activation elicits numerous downstream mitochondrial-metabolic abnormalities and increases fibrogenic cytokine mediators (TGF-β1 and CTGF), which in aggregate promote RV fibrosis. Finally, we show that metabolically targeted therapy reduces RV fibrosis and improves RV function in MCT rats *in vivo*.

METHODS

Extended Methods sections are available in the Online Data Supplement. The authors declare that all supporting data are available within the article and its online supplementary files.

These Methods sections include: reagents, treadmill distance, echocardiography, right heart catheterization, RV-PA coupling, histological analysis, measurement of DCA level in RV tissues, ventricular fibroblasts isolation, cell culture, small interfering RNA treatment on RV fibroblasts, qRT-PCR, sequences for PCR primers and siRNA, microRNA identification, immunoblotting, immunofluorescence on cultured cells, immunofluorescence on tissues, pyruvate dehydrogenase (PDH) enzyme activity, whole cell micropolarimetry, lactate and glucose measurements, mitochondrial morphology, proliferation assay, measurement of mitochondrial reactive oxygen species, measurement of mitochondrial hydrogen peroxide, and determination of sample size in animal study.

Statistical analysis

All of the data are reported as mean ± standard error of the mean (SEM). Two-tailed, Student's *t*-test, paired *t*-test, linear regression analysis, or analysis of variance (ANOVA) was performed as appropriate, after ensuring the data were normally distributed using

Kolmogorov-Smirnov test if the sample size per group is greater than 4. Non-parametric, Mann-Whitney testing was used if the data did not have a normal distribution. The specific test used is listed in the relevant figure legend. Statistical analyses were performed with the GraphPad Prism (GraphPad Software, La Jolla, CA, United States). A *P* value of less than 0.05 was considered statistically significant. All measurements were made by scientists blinded to the treatment groups. Animals were randomized to their respective treatment groups. All analysis was performed with careful attention to blinding of the scientists making the measurements. However, when we could not show all data in the figures (due to space constraints), the representative images of data from cells and tissues were selected to reflect the mean value in the quantitative data, while showing the variability that accounted for the data's standard error.

Monocrotaline-induced PAH animal model

Male Sprague Dawley rats (~250 g; ~7 weeks old) (Charles River, QC, Canada) received a single subcutaneous injection of MCT (60 mg/kg) (n=40) or phosphate buffered saline (PBS; n=21). One week after the injection, rats were randomly assigned to regular drinking water (n=37) or water containing DCA (0.75 g/L; n=24). The estimated average ingestion of DCA was ~25 mg per day per rat. All animals that underwent an endpoint study were included for data analysis and no obtained data were excluded. Female rats display less severe PAH with injection of MCT compared to male rats. Thus, we studied male rats because they have more severe disease. We did not include females because the potential sex difference in RVfib was not the focus of this initial study.

RESULTS

MCT-RVfib have increased PDK expression and decreased PDH activity which is reversed by DCA or the combination of siPDK1 and siPDK3

Compared to control, MCT-RVfib showed an upregulation in the mRNA level of PDK1 and PDK3 (but not PDK2 and PDK4) as well as glucose transporter 1 (Glut1) (Fig. 1A). In contrast, the protein level of PKM1 and PKM2 and the mRNA expression of MPC1 and MPC2 were unchanged (Online Fig. I). We therefore focused on measuring PDK1 and PDK3 protein levels and found that both were upregulated in MCT-RVfib vs. control (Fig. 1B). DCA and isoform-specific siPDK1&3 treatments reduced both mRNA and protein levels of PDK1 and PDK3 in MCT-RVfib (Online Fig. II, Fig. 1B). Neither intervention significantly altered PKM1 or PKM2 (Online Fig. I–A&B). PDH activity was reduced (Online Fig. III) and the ratio of phosphorylated PDH E1-alpha subunit (p-PDH) to total PDH (i.e., p-PDH/total PDH) was increased in MCT-RVfib vs. control (Fig. 1C). In addition, the p-PDH/total PDH ratio was reduced by both DCA and siPDK1&3 treatments, reflecting activation of PDH (Fig. 1C).

MCT-RVfib have a shift from glucose oxidation to uncoupled aerobic glycolysis which is reversed by DCA or the combination of siPDK1 and siPDK3

MCT-RVfib displayed lower oxygen consumption rate (OCR), ATP production, maximum respiration rate, and spare respiration capacity, versus control (Fig. 2A, Online Fig. IV–A). There was no difference in the basal extracellular acidification rate (ECAR; Online Fig. IV–

B); however, the ratio of OCR/ECAR was reduced in MCT-RVfib vs. control (Fig. 2A). Neither DCA nor siPDK1&3 altered mitochondrial metabolism in control-RVfib, but both increased OCR, ATP production, maximum respiration rate, and spare respiration capacity in MCT-RVfib (Fig. 2, Online Fig. IV–A). In addition, both DCA and siPDK1&3 treatments slightly increased the basal ECAR and significantly increased OCR/ECAR in MCT-RVfib (Fig. 2, Online Fig. IV–B). Lactate production and glucose consumption were increased in MCT-RVfib vs. control, and were reduced by both DCA and siPDK1&3 treatments (Fig. 2).

MCT-RVfib display increased mitochondrial fission which is inhibited by DCA or the combination of siPDK 1 and siPDK3

There was increased mitochondrial fission in MCT-RVfib, evident by a significant increase in mitochondrial fragmentation count (MFC) in MCT-RVfib vs. control (Fig. 3A), as previously reported.[41] Both DCA and siPDK1&3 treatments inhibited mitochondrial fission in MCT-RVfib, while having no effect on the control-RVfib (Fig. 3A).

MCT-RVfib display increased rates of proliferation which is reduced by DCA or the combination of siPDK 1 and siPDK3

Compared to control, MCT-RVfib had higher proliferation rate (Fig. 3B) and this persisted for 6 passages in culture (data not shown). Neither DCA nor siPDK1&3 treatment changed the cell proliferation rate in control-RVfib; whereas, both interventions reduced the cell proliferation rate in MCT-RVfib (Fig. 3B). siPDK1 and siPDK3 were tested individually and shown to have >90% knockdown efficiency for their respective PDK isoform mRNA (Online Fig. V). Interestingly, when used separately only siPDK3 reduced proliferation at the dose and duration studied (Fig. 3B).

MCT-RVfib display increased collagen production which is reduced by DCA or the combination of siPDK 1 and siPDK3

Type I and III collagen mRNA (Fig. 4A) and protein (Fig. 4B) were increased in MCT-RVfib vs. control; however, the increase was only statistically significant for type III collagen. Protein levels of type I and III collagen were also confirmed to be increased in MCT-RVfib by immunofluorescence (Online Fig. VI). While neither DCA nor the combination of siPDK1&3 altered the collagen production in control-RVfib, both interventions reduced type I and III collagen in MCT-RVfib (Fig. 4C, Online Fig. VI). Interestingly, when used separately, only siPDK1 (not siPDK3) reduced type I and III collagen production, an effect most evident with type III collagen (Fig. 4D).

MCT-RVfib display decreased MitoSOX levels and this is restored by DCA or the combination of siPDK1 and siPDK3

Compared to control, mitochondrial superoxide (MitoSOX) levels were decreased in MCT-RVfib (Online Fig. VII, Fig. 5A). MitoSOX levels were restored toward normal by both DCA and siPDK1&3 treatments (Fig. 5A, Online Fig. VII). Consistent with MitoSOX production, mitochondria-derived H_2O_2 production was also reduced in MCT-RVfib. As would be expected when reactive oxygen species (ROS) production is increased, mitochondria-derived H_2O_2 production was restored by DCA (Online Fig. VIII Fig. 5A).

MCT-RVfib display normoxic activation of HIF-1α which is reduced by DCA or the combination of siPDK1 and siPDK3

Nuclear HIF-1α, a measure of transcription factor activation, was increased in MCT-RVfib vs. control (Fig. 5B). Both DCA and siPDK1&3 treatments reduced nuclear HIF-1α mRNA level in MCT-RVfib (Fig. 5C).

MCT-RVFib display increased levels of TGF-β1, CTGF and activated dynamin-related protein 1 which are reduced by DCA or the combination of siPDK1 and siPDK3

Activated dynamin-related protein 1 (Drp1) (defined as Drp1 phosphorylated at Serine 616, p-Drp1$_{S616}$) was increased in MCT-RVfib vs. control (Fig. 5D). DCA and siPDK1&3 treatments reduced p-Drp1$_{S616}$ in MCT-RVfib (Fig. 5D). Both TGF-β1 and CTGF protein levels were increased in MCT-RVfib vs. control and were reduced by DCA or siPDK1&3 treatment (Fig. 5E).

DNA methylation activates HIF-1α in MCT-RVfib

Compared to control, MCT-RVfib showed an upregulation in DNMT1 mRNA expression with no changes in DNMT3a and DNMT3b (Online Fig. IX–A). MCT-RVfib showed a downregulation in the mRNA expression of SOD2 (Online Fig. IX–A). These changes were confirmed at the protein level in RVfib using immunofluorescence (Fig. 6A, Online Fig. IX–B). An increase in 5-mc confirmed the global increase in methylation in MCT-RVfib vs. control (Fig. 6B). Conversely, treatment of MCT-RVfib with 5-Azacytidine reduced DNMT1 and 5-mc and restored SOD2 expression (Fig. 6A&B). In addition, reversing DNMT1 activation, using 5-Azacytidine, restored mitochondrial redox signaling in MCT-RVfib. Specifically, 5-Azacytidine restored (increased) MitoSOX and mitochondrial H_2O_2 production (Fig. 6C, Online Fig. X). As expected this restoration of normoxic, mitochondrial redox signaling reduced nuclear HIF-1α in MCT-RVfib (Fig. 6D).

miR-148b-3p was upregulated in MCT-RVfib

To find the potential regulators of DNA methylation, measurement of potential upstream microRNA (miRNA) regulators of DNMT1 was performed (based on predicted or known regulators of DNMT1, as determined by an *in silico* survey using miRWalk 2.0[42] and miRNAs previously shown to be downregulated in PAH in PASMC[43, 44]) (see online supplement). These criteria identified miR-148b-3p as a top hit for negative regulation of DNMT1 and miR-30e-5p as a top hit for negative regulation of DNMT3a. qRT-PCR analysis of both miR-148b-3p and miR-30e-5p reveals that miR-148b-3p was decreased in the MCT-RVfib compared to control whereas miR-30e-5p expression was unchanged (Online Fig. XI). These data suggest miR-148b-3p is the potential induction of increased DNMT1 expression in MCT-RVfib (Fig. 6A). The lack of change in miR-30e-5p (a known regulator of DNMT3a) is consistent with the unchanged DNMT3a expression found in MCT-RVfib (Online Fig. IX–A).

HIF-1α activation increases PDK1 expression in MCT-RVfib

Cobalt treatment of control-RVfib activated HIF-1α and PDK1, but slightly reduced the mRNA expression of PDK3 (Online Fig. XII). Conversely, the treatment of MCT-RVfib with

the HIF-inhibitor, chetomin,[45] reduced the expression of both HIF-1α and HIF-2α mRNA in MCT-RVfib (Online Fig. XIII). Chetomin also reduced the mRNA expression of PDK1, PDK3 and type III collagen in MCT-RVfib (Online Fig. XIII).

Inhibition of DNA methylation restored mitochondrial metabolism and cell function in MCT-RVfib

Inhibiting DNA methylation in MCT-RVfib, using 5-Azacytidine, reduced the expression of PDK1 and the p-PDH/total PDH ratio, and also trended to decrease PDK3 expression (Online Fig. XIV–A, Fig. 6E). 5-Azacytidine also reduced glucose consumption and lactate production and restored OCR (Fig. 6F, Online Fig. XIV–B), indicating the normalization of mitochondrial metabolism in MCT-RVfib. In parallel, mitochondrial dynamics (MFC), rates of cell proliferation, and collagen production were restored toward normal by this DNA methyltransferase inhibitor (Online Fig. XIV–C–E).

DNA methylation mediated, PDK-dependent, depression of mitochondrial metabolism did not occur in MCT-LVfib

The observed phenotype of MCT-RVfib did not occur in MCT-LVfib. Specifically, MCT-LVfib did not display increases in PDK expression nor did they manifest changes in mitochondrial morphology or MitoSOX production, or display the changes in DNMT1, SOD2 or HIF-1α expression (Fig. 6G&H, Online Fig. XV) that were seen in MCT-RVfib. Consistent with the lack of changes in mitochondrial pathways, MCT-LVfib did not have increased rates in cell proliferation, or collagen production relative to control LVfib (Online Fig. XV).

Evidence that DCA therapy achieved effective doses in MCT RV tissues in vivo

DCA-treated MCT RV tissues contained DCA at a range from 0.02 to 0.31 ng/mg, while the RV tissues from MCT rats without DCA treatment did not have detectable levels of DCA (Online Fig. XVI, Fig. 7A). p-PDH in fibroblasts was increased in MCT RV tissues and these levels were restored toward normal by DCA therapy (Fig. 7B).

In MCT rats increased RV fibrosis were improved by DCA

Compared to control, RVs from MCT rats exhibited significantly more collagen deposition (Fig. 7C). In contrast, collagen deposition in the LV was not significantly different between MCT and control (PBS) groups (Fig. 7C). While DCA had no effect on the collagen deposition in the control RVs, it reduced the collagen deposition in the RVs from MCT rats (Fig. 7C).

Increased RV fibrosis and PDK1 expression in RVfib were observed in PAH patients

RVs from PAH patients with decompensated RV failure displayed greater RV fibrosis versus control subjects (Fig. 7D). While PDK1 expression in RVfib was increased in PAH patients, there was no significant change in PDK3 expression in PAH RVfib (Fig. 7E).

In MCT rats reduced RV function was improved by DCA

At week-4 post-injection of MCT or PBS, body weight was significantly less in MCT vs. control rats (365 ± 7 g vs. 488 ± 14 g, $P=1.1\times10^{-12}$) and was not altered by DCA treatment (361 ± 9 g for MCT+DCA rats and 435 ± 10 g for PBS+DCA rats). MCT rats had significantly increased PA and RV pressures versus control [mPAP: 41 ± 2.0 vs. 13 ± 0.6 mmHg, RV systolic pressure (RVSP): 61 ± 3.0 vs. 18 ± 0.9 mmHg, and RV end-diastolic pressure (RVEDP): 16 ± 2.0 vs. 5.4 ± 0.4 mmHg; Fig. 8A, Online Fig. XVII]. DCA treatment reduced both PA and RV pressures in MCT rats (mPAP: 25 ± 2.0 mmHg, RVSP: 43 ± 4.0 mmHg, and RVEDP: 10 ± 1.0 mmHg; Fig. 8A). Consistent with RHC, echocardiography showed that compared to control, MCT rats had shorter PA acceleration time (PAAT) than control (16 ± 0.8 vs. 32 ± 0.8 ms), and this was improved by DCA (23 ± 1.4 ms) (Fig. 8B). In addition, MCT caused RVH, evident as increased RV free wall (RVFW) diastolic thickness (1.35 ± 0.04 vs. 0.61 ± 0.04 mm; Fig. 8B) and Fulton index (RV/LV+S) (0.63 ± 0.02 vs. 0.28 ± 0.01; Fig. 8C). DCA reduced RVH in MCT rats (RVFW diastolic thickness: 0.88 ± 0.10 mm and RV/LV+S: 0.49 ± 0.04; Fig. 8B&C). Moreover, RV systolic function, indicated by RVFW systolic thickening and TAPSE, was reduced in MCT rats compared to control (RVFW thickening: 25 ± 5 vs. 102 ± 3 and tricuspid annular plane systolic excursion, TAPSE: 1.9 ± 0.1 vs. 3.2 ± 0.1 mm; Fig. 8B) and improved by DCA in MCT rats (RVFW thickening: 71 ± 10 and TAPSE: 2.3 ± 0.2 mm; Fig. 8B). Compared with control, MCT rats had reduced cardiac output (CO; 66 ± 10 vs. 147 ± 7 mL/min) and ran for a shorter distance in the treadmill test (20 ± 7 vs. 256 ± 23 m). Both CO and the maximum running capacity were improved by DCA (CO: 96 ± 10 mL/min and treadmill distance: 60 ± 19 m; Fig. 8B&C).

RV-PA coupling

To apportion the relative contributions of improved RV function versus regression of pulmonary vascular disease to the observed benefit accrued by MCT+DCA rats, we analyzed the RV-PA coupling. Both the measures of RV-PA coupling (i.e., TAPSE/mPAP and RVFW thickening/mPAP ratios) were reduced significantly in MCT rats vs. the control and were partially recovered by DCA treatment (Fig. 8D). In addition, there were strong inverse relationships between TAPSE and mPAP (R^2=0.81, P=0.000027) and between RVFW thickening and mPAP (R^2=0.78, P=0.000059) in PBS and MCT groups (Online Fig. XVIII–A). In the MCT+DCA rats, however, there was a slightly positive slope in the TAPSE vs. mPAP relationship (R^2=0.30, P=0.27) and an inverse, but less steep, slope in the RVFW thickening vs. mPAP relationship (R^2=0.14, P=0.47) as compared to that in PBS and MCT groups (Online Fig. XVIII–A). The loss of the strong inverse relationship in MCT+DCA rats indicates improved RV function by DCA. A schematic plot for the relationship between TAPSE or RVFW thickening and mPAP is shown in Online Fig. XVIII–B. While PBS and MCT rats fall on the solid line, the DCA-treated MCT rats fall on the dashed-blue line with less steep slope (i.e., reduced inclination). This plot shows that while DCA treatment reduces mPAP or PVR, indirectly improving RV function, it also directly improves RV function and RV-PA coupling.

DISCUSSION

RV fibrosis occurs in RVF. While the role of RV fibrosis in the development of RVF remains speculative,[46] it is well established that the mortality rates from RVF exceed 40% for hospitalized PAH patients.[47, 48] Thus, improved mechanistic understanding of the basis for RV fibrosis and RVF and identification of antifibrogenic therapies have great potential impact. Warburg metabolic remodeling has been shown to be activated in many disease-relevant cell types in PAH, including PASMC, PAEC, PAfib and RV cardiomyocytes. However, this is the first study to identify the occurrence of this pathway in RVfib in experimental and human PAH. Moreover, we show the consequences of this pathway, linking it directly to increased fibroblast proliferation and collagen production. This leads to potential translational applications, namely metabolic modulation to reduce RV fibrosis. We also show for the first time that this PDK-mediated modulation has different isoform specificity in RVfib than in RV cardiomyocytes (PDK1&3 versus PDK2&4), which may have therapeutic implications. Finally, we identify the basis for this metabolic reprogramming of RVfib, demonstrating that epigenetic pathways, involving miRNAs and DNMT1, are upstream of the metabolic changes, and elicit these changes through altered mitochondrial redox signaling.

Thus, this study offers many new findings:

1. First, while our group and others have established the pathologic role of altered epigenetics and disordered mitochondrial metabolism in pulmonary vascular cells and RV cardiomyocytes in PAH, little was previously known about the role of either epigenetic reprogramming or Warburg metabolism in PAH RVfib. We show that the upregulation of PDK isoforms 1 and 3 and the resulting PDH inhibition contributes to the hyperproliferative, fibrogenic Warburg phenotype in RVfib. Unlike findings in PAfib, we found no alterations of PKM2/PKM1.[25]

2. Second, we show that it is the acquired epigenetic changes in mitochondrial redox signaling leading to persistent metabolic changes in RVfib that drive their rate of proliferation and collagen production. This epigenetic reprogramming is mediated by upregulation of DNMT1. DNMT1 increases DNA methylation in RVfib and this impairs transcription of many genes, including (relevant to this study) SOD2.

3. Third, we show that DNMT1 impairs mitochondria redox signaling by impairing SOD2-mediated production of H_2O_2, creating a state of *pseudohypoxia* that leads to normoxic HIF-1α activation, as previously reported in PAH PASMC.[38]

4. We show for the first time that this epigenetic activation of HIF-1α, a known transcriptional regulator of PDK[37, 49–51], drives the Warburg metabolic shift. HIF-1α, also elevates production of fibrogenic cytokines (CTGF and TGF-β1), increases mitochondrial fission, which drives proliferation and collagen production in MCT-RVfib. The MCT-RVfib's hyperproliferative, fibrogenic phenotype persists in culture, consistent with prior observations of a persistent proliferative phenotype in RVfib from Sugen-Hypoxia rats.[20]

5. This study shows that PAH RVfib share the Warburg metabolic shift seen in other disease-relevant cells in PAH. Based on expression profiling and siRNA studies, only isoforms 1 & 3 underlie the inhibition of PDH activity and the reduced OCR/ECAR ratio and increased lactate production in MCT-RVfib. These metabolic modifications are therapeutically relevant since chemical or molecular inhibition of PDK 1 and 3 reduces mitochondrial fission, proliferation and collagen production in MCT-RVfib.

6. In human PAH, PDK1 expression is markedly increased in RVfib, supporting the translational relevance of our findings and suggesting PDK1, which is most upregulated in MCT-RVfib, may also be the most disease relevant PDK isoform in RVfib of PAH patients.

7. We documented that DCA as administered *in vivo* led to measurable RV concentrations of DCA, using mass spectrometry measurements (Fig. 7A). These levels were effective, evident from the observed decrease in phospho-PDH in the RV (Fig. 7B).

8. Finally, while DCA benefits both the lung circulation and RV, we show that it improves RV-PA coupling, suggesting at least part of its beneficial effect related to a direct improvement in RV function. This has clinical implications as RV fibrosis is not targeted by current PAH therapies and PAH patients die of RV failure.

In the MCT model, HIF1-α increases PDK expression and also activates fibrogenic cytokines (CTGF and TGF-β1) which, in combination cause the MCT-RVfib to proliferate and produce collagen at pathologic rates. Elevated expression of DNMT1, a methyltransferase which conveys epigenetic methylation that is resilient, persisting through mitosis to imprint daughter cells, leads to increased DNA methylation that persists in RVFib passaged in cell culture. Although we did not do a whole methylome survey, we show that DNMT1 decreases SOD2 expression thereby reducing production of mitochondrial-derived superoxide and H_2O_2. This reduced environment leads to normoxic activation of HIF-1α.[38] HIF1-α is a known transcriptional activator of certain PDK isoforms, including PDK1.[37] This DNMT1-SOD2-HIF-1α-PDK pathway is similar to that described in PASMC,[38] but in RVfib, HIF-1α also increases TGF-β1- and CTGF- mediated collagen production and fibrosis. This fibrogenic pathway activation is chamber-specific and is not seen in the MCT-LVFib, arguing that it is not simply a nonspecific response to exposure to MCT. This discovery has therapeutic implications as PDK inhibition reduces RV fibrosis and improves RV function in MCT rats *in vivo.*

The metabolic theory of PAH proposes that acquired inhibition of mitochondrial glucose oxidation occurs in vascular cells and RV cardiomyocytes in human and experimental PAH. [52, 53] Although mitochondrial metabolic abnormalities have previously been reported in PASMC,[24] PAEC,[28, 29] PAfib[25–27] and RV cardiomyocytes[13, 30, 54] in PAH, the mitochondrial metabolic profile of RVfib and its potential role in RV fibrosis was largely unknown. In a recent study, we showed that RVfib isolated from the RVs of rats with MCT-induced PAH have a hyperproliferative phenotype that persists in culture.[41] This phenotype was marked by mitochondrial fragmentation due to increased Drp1-mediated mitochondrial

fission. Inhibiting Drp1-mediated mitotic fission reduced RVfib proliferation and decreased collagen production. However, neither the relationship between fission and metabolism nor the basis for the persistence of this phenotype in culture was evaluated. In the current study we show that Drp1 activation and the resulting fragmented mitochondrial phenotype is downstream from the DNMT1-mitochondrial redox signalling-HIF-1α pathway, and is corrected by *in vitro* therapy with 5-Azacytidine.

Glucose is transported into the cytosol by glucose transporters (Glut1 and Glut4). Whereupon it is metabolized by glycolysis to form pyruvate. The terminal step in glycolysis is catalyzed by PK (i.e., the PKM2/PKM1 ratio), pyruvate is either converted to lactate or transported into mitochondria via the MPC subunits 1 and 2 (MPC1 and MPC2, respectively).[25] Within the mitochondrial matrix pyruvate is oxidized by PDH to form acetyl coenzyme A, which feeds Krebs' cycle. This pathway can be interrupted at multiple levels in PAH, in manners that vary amongst cell types. Increased uncoupled aerobic glycolysis can reflect the following abnormalities, alone or in combinations: PDK-mediated PDH inhibition, increased PKM2/PKM1 ratio, and reduced expression of MPC1 and MPC2.[55] Unlike the recent findings in PAfib[25] and PAEC[28], the Warburg metabolic shift in MCT-RVfib was not associated with changes in the PKM2/PKM1 ratio or expression of the MPCs (Online Fig. I). Rather, we found that as in PASMC[24] and RV cardiomyocytes[33] the metabolic shift was due to increased PDK expression (Fig. 1).

The predominant PDK isoforms differ in RVfib vs. cardiomyocytes. Whilst PDK2 and PDK4 are increased in RV cardiomyocytes from Fawn-hooded rat model of PAH,[33] PDK1 and PDK3 are the predominant isoforms in MCT-RVfib (Fig. 1A). There is some heterogeneity in the expression and function of PDK1 and PDK3. For example, PDK3 expression is increased relatively more than PDK1 in MCT vs. control RVfib (Fig. 1B). Moreover, whilst DCA treatment reduces PDK1 in the MCT group to levels near those of the control group, it only partially reduces PDK3 expression (Fig. 1B). This likely reflects the heterogeneous isoform sensitivity of DCA for PDK. For example, 8-fold higher concentrations of DCA are required to inhibit PDK3 (K_i=8 mM), as compared to PDK1 (K_i=1 mM).[56] In addition, experiments using isoform-specific siPDKs show that PDK1 and PDK3 differentially regulate proliferation and collagen production (Fig. 3B, Fig. 4D), with siPDK1 having a greater effect on collagen production and siPDK3 having a greater effect on fibroblast proliferation. The molecular mechanisms and downstream targets underlying this PDK isoform heterogeneity in biological activity are currently unknown. The consequences of PDK upregulation included increased PDH phosphorylation and reduced PDH activity (Fig. 1C, Online Fig. III), which is also observed in RV cardiomyocytes,[33] PASMC[24] and PAfib[25, 27] in PAH.

We next investigated the cause of PDK upregulation in MCT-RVfib. In the PAH PASMC, activation of DNMT1 and DNMT3b methylates the SOD2 promoter resulting in reduced SOD2 expression.[38] Similarly, we noted reduced SOD2 expression and MitoSOX and mitochondrial H_2O_2 levels in MCT-RVfib (Fig. 5A, Fig. 6A). It has been shown by several groups that low SOD2 levels activate HIF-1α, although the effects on superoxide radicals and peroxides production varies between studies.[38, 57] Compared to control, MCT-RVfib showed activation in HIF-1α (Fig. 5B) that was associated with reduced mitochondrial

superoxide and mitochondrial H_2O_2 levels (Fig. 5A) and decreased SOD2 expression (Fig. 6B). Proof that this reflects methylation related processes is the observation that 5-Azacytidine restored SOD2 expression and increased mitochondrial superoxide and mitochondrial H_2O_2 levels (Fig. 6A&C) and reduced nuclear (activated) HIF-1α expression (Fig. 6D). These epigenetic signals, acquired *in vivo* as a consequence of exposure to MCT, can be passed to daughter cells through replication by means of DNMT1. This explains the persistence of the mitochondrial metabolic phenotype in cell culture, despite multiple passages. Indeed, we show that the increases in DNA methylation (5-mc levels) in the nuclei of MCT-RVfib are reversed by 5-Azacytidine (Fig. 6B).

The PDK mediated inhibition of PDH impairs Krebs' cycle and resulted in the reduction in OCR (Fig. 2). As expected, this was accompanied by higher glucose uptake in MCT-RVfib, reflecting a compensatory increase in uncoupled glycolysis, and increased lactate production. This pattern of enhanced glycolysis and impaired glucose oxidation has previously been reported in PA vascular cells and RV cardiomyocytes both in animal models of PAH and PAH patients,[24, 27, 33, 39] and in RV and lung in animal models of PAH and PAH patients.[15, 16, 24, 30, 33, 36, 39]

We identified three consequences of Warburg metabolism in MCT-RVfib. First, the change in metabolism promotes increased mitochondrial fission (Fig. 3A). This is consistent with changes seen in other cell types in PAH, e.g., RV cardiomyocytes,[58] PASMC,[44, 45, 59] and PAfib.[27] It is possible that this mitochondrial fragmentation simply reflects the increase in rates of mitotic fission required to support a metabolism-induced increase in cell proliferation rates. Mitochondrial division is thought to coordinate the division of the nucleus and the mitochondria and thus increased mitochondrial fission both reflects, and is required to support, rapid cell proliferation.[44, 45] Second, the metabolically remodeled RVfib are highly proliferative (Fig. 3B). Interestingly the proliferative effect of uncoupled glycolytic metabolism was observed by Warburg himself in cancer cells.[60] The third consequence is that MCT-RVfib produce more type III collagen (Fig. 4). At baseline in normal fibroblasts type I collagen is the predominant form (Fig. 4). Interestingly RVfib from Sugen-Hypoxia rats exhibited a significant increase in type I collagen[20]. This primacy of type III collagen expression (in our study) could be due to the different PAH models used, although we also found a trend toward increased type I collagen. Importantly the metabolic changes increased expression of major mediators known to promote collagen production namely, CTGF and TGF-β 1.

A testimony to the plasticity of the RVfib in PAH is that restoring glucose oxidation via inhibiting PDK restores the RVfib's mitochondrial network (Fig. 3A), reduces RVfib proliferation (Fig. 3B), and reduces collagen production both in cell culture and *in vivo* (Fig. 4, Fig. 7C). These improvements in RVfib function can be achieved by inhibition of PDK isoforms 1 and 3 (Figs. 2–4) or by upstream targeting of HIF-1α (Fig. 5). HIF-1α activation is known to cause mitochondrial fission and promote to cell proliferation in PAH PASMC [45]. HIF-1α activation also increases collagen production by a TGF-β1- and CTGF-dependent mechanism in lung and kidney epithelial cells.[61–63] PDK inhibition not only improves mitochondrial metabolism (Fig. 2), but also restores mitochondrial superoxide and mitochondrial H_2O_2 levels (Fig. 5A) and reduces HIF-1α activation (Fig. 5C). PDK

inhibition (by decreasing nuclear HIF-1α expression) reduces mitochondrial fission by decreasing levels of activated Drp1 (p-Drp1$_{S616}$) (Fig. 5D) while simultaneously reducing fibrosis, by decreasing TGF-β1 and CTGF expression (Fig. 5E). These molecular changes underlie the therapeutic benefits of DCA or siPDK1&3 that we observed (Figs. 3&4).

DCA has a very specific mechanism in inhibiting PDK, namely it mimics pyruvate's structures and competes with pyruvate in PDK's binding pocket, resulting in PDK inhibition.[34] Thus DCA is a specific PDK inhibitor and does not directly target cytokines. Rather, in MCT-RVfib, PDK upregulation reduced glucose oxidation (Fig. 2), reducing mitochondrial superoxide (Online Fig. VII, Fig. 5A) and H_2O_2 (Online Fig. VIII, Fig. 5A) production by the electron transport chain. These redox changes activate HIF-1α which upregulates TGF-β1 and CTGF,[61–63] leading to increased collagen production and fibrosis. Conversely, DCA inhibits PDK (Fig. 1), restores mitochondrial redox signaling, inactivates HIF-1α (Fig. 5), and through this mechanism decreases the expression of TGF-β1 and CTGF (Fig. 5E) and collagen production (Fig. 4). Therefore, our data suggest the reduced TGF-β1 and CTGF following DCA therapy reflects restoration of PDH-dependent glucose oxidation.

As expected, RV from MCT rats manifested a chamber specific increase in fibrosis (Fig. 7B) and ventricular dysfunction *in vivo* (Fig. 8), consistent to the observed fibrosis in the decompensated RV from PAH patients (Fig. 7D). RV fibrosis and dysfunction in PAH have been previously shown to occur in MCT and Sugen-Hypoxia rats and PAH patients.[12, 17–20] As RV afterload increases during the progression of PAH, RV contractile function is impaired (reduced TAPSE, RVFW thickening, and CO) and RV diastolic function is also impaired (increased RVEDP), resulting in functional impairment (reduced treadmill distance) (Fig. 8). The increased RVEDP is due to increased stiffness of RV, which likely reflects both impairment of active lusitropic properties of the RV (such as altered t-tubule structure due to impaired expression of junctophilin 2)[64] and the more passive consequences of increased RV fibrosis.

In LV, we did not find fibrosis in MCT rats (Fig. 7C), consistent with previous studies.[19, 65] This is not surprising since there was no increase in the expression of DNMT1, SOD2, HIF-1α, or PDK isoforms in MCT-LVfib (Fig. 6G&H, Online Fig. XV), consistent with our previous finding that LV in MCT rat does not have changes in the expression of Glut1 or phosphorylated PDH or increased glucose uptake, as measured using fluorodeoxyglucose PET.[30] Lacking the epigenetic-metabolic derangement of RVfib, it follows that there is no change in mitochondrial morphology, cell proliferation rate or collagen production in MCT-LVfib.

In vivo, DCA treatment restores RV glucose oxidation, reverses PA remodeling and improves hemodynamics and survival rate in MCT rats[24, 30, 40] and improves hemodynamics and survival rate in Fawn-hooded rats.[33] These benefits have previously been assumed to result from regression of pulmonary vascular obstruction[40] and enhanced RV contractility.[30] In addition to these benefits, we provide new evidence that DCA also reduces RV fibrosis (Fig. 7C). In an attempt to attribute the relative cause of improved pulmonary vascular function vs. RV function, we performed the RV-PA coupling analysis. The increase in RV-

PA coupling (indicated by the TAPSE/mPAP and RVFW thickening/mPAP ratios) and the altered TAPSE vs. mPAP and RVFW thickening vs. mPAP relationships observed in DCA-treated in MCT rats (Fig. 8D, Online Fig. XVIII) suggests improvement in RV systolic function contributed to the net benefit, in addition to the benefits in the pulmonary vasculature (e.g. reduced mPAP) (Online Fig. XVIII–B).

DCA is a specific, but not a potent, PDK inhibitor. DCA also has variable sensitivity for the 4 PDK isoforms, evident from K_i values of 1.0, 0.2, 8.0 and 0.5 mM for PDK1, PDK2, PDK3 and PDK4, respectively.[56] Because of DCA's low potency, the *in vitro* concentration used (by us and others) is in the mM range, ensuring effective inhibition of all PDK isoforms. The dose of DCA in the *in vitro* study is high primarily because the treatment with DCA is brief. *In vivo* we believe DCA's effects accumulate over time and the efficacy of the dose we used is supported by the observation that RV phospho-PDH expression fell in DCA-treated MCT RVs (Fig. 7B). Moreover, we measured DCA concentration in the RV *in vivo* using mass spectrometry. The amount of DCA in RV tissues of DCA-treated MCT rats (Fig. 7A) is in the therapeutic range based on prior study.[34] The PDK isoforms that are most important to RV fibrosis, based on their increased expression and the therapeutic effects of highly isoform specific siRNA, are PDK1 and 3. It appears that inhibiting PDK1 and PDK3 in combination reduces fibroblast proliferation and collagen production, although there may be differential effect of the two isoforms for these functions (Fig. 3B&4D).

To address the translational implications of the PDK pathway in MCT-RVfib, we decided to use human PAH RV samples, rather than study another rodent model. We evaluated the expression of PDK in RVfib of control subjects and subjects with RVF due to PAH (Fig. 7E). In these blinded studies of human RVs, fibroblasts were identified by positive staining for vimentin. Compared to RVfib in control subjects, PAH-RVfib in patients (vimentin-positive fibroblasts) have a marked upregulation of PDK1. While PDK3 is strongly expressed in the PAH RVfib it is not upregulated relative to control. Thus, we conclude PDK1 is the predominant isoform involved in the fibrogenic pathway in patients and rodents and the role of PDK3 is relevant but likely smaller (Fig. 3B&4D).

Limitations

Several limitations are acknowledged. First, we recognize that the observed improvement in RV function with DCA is likely a reflection of DCA's known ability to cause beneficial pulmonary vascular remodeling and improve RV cardiomyocyte bioenergetics, in addition to the new observation of a reduction in RV fibrosis. DCA treatment improves RV contractility in MCT rats (Fig. 8B) and in *ex vivo* Langendorff RV model,[30] indicating its ability to directly improve RV contractility. The change in RV-PA coupling we observed (Fig. 8D, Online Fig. XVIII) suggests that DCA has additional beneficial effects on the RV, independent of its important beneficial effects on the pulmonary vasculature. A direct improvement in RV function has also been shown to occur with DCA treatment in the pulmonary artery banding rat model,[30] a model in which there is no pulmonary vascular disease. While it is now clear that DCA also reduces RV fibrosis (Fig. 7C), we cannot distinguish the precise contribution of improved RV contractility vs. reduced RV fibrosis to the improved RV function observed in DCA-treated MCT rats.

Second, several recent studies using the anti-fibrotic agent, pirfenidone, found that it reduced RV fibrosis in PAB mice[66] but not in PAB rats.[46] Surprisingly, pirfenidone did not improve RV function in either PAB mice or rats.[46, 66] The lack of improvement in RV function in PAB mice treated with pirfenidone may indicate that reducing fibrosis alone, without simultaneously addressing other RV maladaptations (metabolic remodeling with impaired inotropy, reduced capillary and inflammation), is insufficient.[67] The precision of the pirfenidone approach contrasts with multipronged benefits of PDK inhibition we employed.

In addition, cell-cell interaction is important to RV function, as RV fibroblasts can release paracrine factors that drive RV cardiomyocyte dedifferentiation, likely leading to RV dysfunction.[68] In other words, simply reducing collagen production using pirfenidone, may be inferior to metabolic therapies that improve several fibroblast functions, such as mitochondrial metabolism, redox signaling and dynamics. The relative benefits of metabolic vs. fibrosis-specific therapies will require direct investigation, and was not performed in the current study.

We did not study RVfib from Sugen-Hypoxia rats. The fact is that no single animal model can capture all the features of human PAH.[69] While Sugen-Hypoxia rats display plexiform lesion in PA in the lung, a key feature of human PAH, MCT rats develop RVF, consistent with patients with PAH with RV decompensation. Nevertheless, studying this epigenetic pathway in RVfib from Sugen-Hypoxia rats and PAH patients would be an important future direction of study.

The maximal respiration rate and spare respiration capacity were also reduced in MCT-RVfib (Online Fig. IV). These changes in mitochondrial respiration in MCT-RVfib likely indicate abnormalities in mitochondrial electron transport chain complexes I, III and/or IV. Indeed, decreased Complex I or IV activity have been observed in PASMC[35, 70], PAfib[27] or PAEC[39] in PAH. Changes in the function/expression of these complexes in RVfib require further study.

In addition, there are certainly multiple pathways dysregulated in MCT-RVfib. Many of these will be epigenetically regulated. In future studies we will layer transcriptomic data (identifying pathway dysregulation) with methylomic data (identifying genes that are differentially methylated in the MCT RV) to determine the role of methylome in RV fibrosis. Even this will not complete the task, as other methylation-independent epigenetic mechanisms, relating to histone modification and miRNAs, are likely also participatory. Thus the field of epigenetic regulation of fibrosis will likely be a profitable area of investigation for years to come.

Finally, HIF-1α has been found to play a role in glutamine metabolism. Glutaminolysis is induced in experimental RVH, and has a reciprocal relationship with glucose oxidation in the RV.[13] This remains a subject for future study.

Conclusions

This study highlights the pathological importance of epigenetically-mediated, mitochondrial redox-regulated, HIF-1α-dependent, PDK1&3-mediated, induction of a Warburg metabolic

phenotype in RVfib. It also demonstrates the potential pathological and therapeutic relevance of this pathway for RV fibrosis in PAH (Fig. 8E). This pathway suggests new therapeutic approaches, including inhibition of DNMT1 or isoform-specific PDK inhibitors. We can now add the RVfib to the list of cells in PAH that have a shared Warburg metabolic basis for dysfunction in PAH, namely, all cells in the pulmonary vasculature (PASMC, PAfib and PAEC) and RV cardiomyocytes. Thus, metabolic therapies which reverse the Warburg metabolic phenotype are anticipated to be beneficial to all cells in the cardiopulmonary unit. This work establishes the epigenetic basis for RV fibrosis and demonstrates that it is therapeutically tractable.

Supplementary Material

Refer to Web version on PubMed Central for supplementary material.

ACKNOWLEDGEMENTS

Nonstandard Abbreviations and Acronyms

5-mc
5-methylcytosine

CO
cardiac output

CTGF
connective tissue growth factor

DCA
sodium dichloroacetate

DNMT1, DNMT3a or DNMT3b
DNA methyltransferase 1, 3a or 3b, respectively

Drp1
dynamin-related protein 1

ECAR
extracellular acidification rate

Glut1 or Glut4

glucose transporter 1 or 4

HIF-1α
hypoxia-inducible factor 1 alpha

LV
left ventricle

LVfib
left ventricular fibroblasts

LV+S
left ventricle plus septum

MCT
monocrotaline

MFC
mitochondrial fragmentation count

miRNA
microRNA

MitoSOX
mitochondrial superoxide

mPAP
mean pulmonary artery pressure

MPC1 or MPC2
mitochondrial pyruvate carrier 1 or 2

OCR
oxygen consumption rate

PA
pulmonary artery

PAAT
pulmonary artery acceleration time

PAEC
pulmonary artery endothelial cells

PAfib
pulmonary artery adventitial fibroblasts

PAH
pulmonary arterial hypertension

PASMC
pulmonary artery smooth muscle cells

PDH
pyruvate dehydrogenase

PDK1, PDK2, PDK3 or PDK4
pyruvate dehydrogenase kinase isoform 1, 2, 3, or 4

PK
pyruvate kinase

PKM1 or PKM2
pyruvate kinase muscle isoform 1 or 2

p-Drp1$_{S616}$
phosphorylated dynamin-related protein 1 at Serine 616

p-PDH
phosphorylated pyruvate dehydrogenase

PTBP1
polypyrimidine tract-binding protein 1

PVR
pulmonary vascular resistance

RHC
right heart catheterization

ROS
reactive oxygen species

RV
right ventricle

RVEDP
right ventricular end-diastolic pressure

RVF
right ventricular failure

RVfib
right ventricular fibroblasts

RVFW
right ventricular free wall

RVH
RV hypertrophy

RVSP

right ventricular systolic pressure

siPDK1

small interfering RNA targeting pyruvate dehydrogenase kinase isoform 1

siPDK3

small interfering RNA targeting pyruvate dehydrogenase kinase isoform 3

siPDK1&3

small interfering RNA targeting pyruvate dehydrogenase kinase isoforms 1 and 3

SOD2

superoxide dismutase 2

TAPSE

tricuspid annular plane systolic excursion

TGF-β1

transforming growth factor beta-1

REFERENCES

1. Sandoval J, Bauerle O, Palomar A, Gomez A, Martinez-Guerra ML, Beltran M and Guerrero ML. Survival in primary pulmonary hypertension. Validation of a prognostic equation. Circulation. 1994;89:1733–44. [PubMed: 8149539]

2. D'Alonzo GE, Barst RJ, Ayres SM, Bergofsky EH, Brundage BH, Detre KM, Fishman AP, Goldring RM, Groves BM, Kernis JT and et al. Survival in patients with primary pulmonary hypertension. Results from a national prospective registry. Ann Intern Med. 1991;115:343–9. [PubMed: 1863023]

3. Campo A, Mathai SC, Le Pavec J, Zaiman AL, Hummers LK, Boyce D, Housten T, Champion HC, Lechtzin N, Wigley FM, Girgis RE and Hassoun PM. Hemodynamic predictors of survival in scleroderma-related pulmonary arterial hypertension. Am J Respir Crit Care Med. 2010;182:252–60. [PubMed: 20339143]

4. Ghio S, Klersy C, Magrini G, D'Armini AM, Scelsi L, Raineri C, Pasotti M, Serio A, Campana C and Vigano M. Prognostic relevance of the echocardiographic assessment of right ventricular function in patients with idiopathic pulmonary arterial hypertension. International journal of cardiology. 2010;140:272–8. [PubMed: 19070379]

5. Humbert M, Sitbon O, Chaouat A, Bertocchi M, Habib G, Gressin V, Yaici A, Weitzenblum E, Cordier JF, Chabot F, et al. Survival in patients with idiopathic, familial, and anorexigen-associated pulmonary arterial hypertension in the modern management era. Circulation. 2010;122:156–63. [PubMed: 20585011]

6. Sachdev A, Villarraga HR, Frantz RP, McGoon MD, Hsiao JF, Maalouf JF, Ammash NM, McCully RB, Miller FA, Pellikka PA, Oh JK and Kane GC. Right ventricular strain for prediction of survival in patients with pulmonary arterial hypertension. Chest. 2011;139:1299–1309. [PubMed: 21148241]

7. Voelkel NF, Bogaard HJ and Gomez-Arroyo J. The need to recognize the pulmonary circulation and the right ventricle as an integrated functional unit: facts and hypotheses (2013 Grover Conference series). Pulmonary circulation. 2015;5:81–9. [PubMed: 25992273]

8. Ryan JJ and Archer SL. The right ventricle in pulmonary arterial hypertension: disorders of metabolism, angiogenesis and adrenergic signaling in right ventricular failure. Circulation research. 2014;115:176–88. [PubMed: 24951766]

9. Bristow MR, Ginsburg R, Umans V, Fowler M, Minobe W, Rasmussen R, Zera P, Menlove R, Shah P, Jamieson S and et al. Beta 1- and beta 2-adrenergic-receptor subpopulations in nonfailing and

failing human ventricular myocardium: coupling of both receptor subtypes to muscle contraction and selective beta 1-receptor down-regulation in heart failure. Circulation research. 1986;59:297–309. [PubMed: 2876788]

10. Vlahakes GJ, Turley K and Hoffman JI. The pathophysiology of failure in acute right ventricular hypertension: hemodynamic and biochemical correlations. Circulation. 1981;63:87–95. [PubMed: 7438411]

11. van Wolferen SA, Marcus JT, Westerhof N, Spreeuwenberg MD, Marques KM, Bronzwaer JG, Henkens IR, Gan CT, Boonstra A, Postmus PE and Vonk-Noordegraaf A. Right coronary artery flow impairment in patients with pulmonary hypertension. Eur Heart J. 2008;29:120–7. [PubMed: 18065750]

12. Bogaard HJ, Natarajan R, Henderson SC, Long CS, Kraskauskas D, Smithson L, Ockaili R, McCord JM and Voelkel NF. Chronic pulmonary artery pressure elevation is insufficient to explain right heart failure. Circulation. 2009;120:1951–60. [PubMed: 19884466]

13. Piao L, Fang YH, Parikh K, Ryan JJ, Toth PT and Archer SL. Cardiac glutaminolysis: a maladaptive cancer metabolism pathway in the right ventricle in pulmonary hypertension. Journal of molecular medicine. 2013;91:1185–97. [PubMed: 23794090]

14. Potus F, Ruffenach G, Dahou A, Thebault C, Breuils-Bonnet S, Tremblay E, Nadeau V, Paradis R, Graydon C, Wong R, et al. Downregulation of MicroRNA-126 Contributes to the Failing Right Ventricle in Pulmonary Arterial Hypertension. Circulation. 2015;132:932–43. [PubMed: 26162916]

15. Oikawa M, Kagaya Y, Otani H, Sakuma M, Demachi J, Suzuki J, Takahashi T, Nawata J, Ido T, Watanabe J and Shirato K. Increased [18F]fluorodeoxyglucose accumulation in right ventricular free wall in patients with pulmonary hypertension and the effect of epoprostenol. J Am Coll Cardiol. 2005;45:1849–55. [PubMed: 15936618]

16. Basu S, Alzeair S, Li G, Dadparvar S and Alavi A. Etiopathologies associated with intercostal muscle hypermetabolism and prominent right ventricle visualization on 2-deoxy-2[F-18]fluoro-D-glucose-positron emission tomography: significance of an incidental finding and in the setting of a known pulmonary disease. Mol Imaging Biol. 2007;9:333–9. [PubMed: 17610018]

17. Lowes BD, Minobe W, Abraham WT, Rizeq MN, Bohlmeyer TJ, Quaife RA, Roden RL, Dutcher DL, Robertson AD, Voelkel NF, et al. Changes in gene expression in the intact human heart. Downregulation of alpha-myosin heavy chain in hypertrophied, failing ventricular myocardium. J Clin Invest. 1997;100:2315–24. [PubMed: 9410910]

18. Nadadur RD, Umar S, Wong G, Eghbali M, Iorga A, Matori H, Partow-Navid R and Eghbali M. Reverse right ventricular structural and extracellular matrix remodeling by estrogen in severe pulmonary hypertension. J Appl Physiol (1985). 2012;113:149–58. [PubMed: 22628376]

19. Umar S, Lee JH, de Lange E, Iorga A, Partow-Navid R, Bapat A, van der Laarse A, Saggar R, Saggar R, Ypey DL, Karagueuzian HS and Eghbali M. Spontaneous ventricular fibrillation in right ventricular failure secondary to chronic pulmonary hypertension. Circ Arrhythm Electrophysiol. 2012;5:181–90. [PubMed: 22199010]

20. Gomez-Arroyo J, Sakagami M, Syed AA, Farkas L, Van Tassell B, Kraskauskas D, Mizuno S, Abbate A, Bogaard HJ, Byron PR and Voelkel NF. Iloprost reverses established fibrosis in experimental right ventricular failure. Eur Respir J. 2015;45:449–62. [PubMed: 25261325]

21. Andersen S, Nielsen-Kudsk JE, Vonk Noordegraaf A and de Man FS. Right Ventricular Fibrosis. Circulation. 2019;139:269–285. [PubMed: 30615500]

22. Freed BH, Gomberg-Maitland M, Chandra S, Mor-Avi V, Rich S, Archer SL, Jamison EB Jr.,, Lang RM and Patel AR. Late gadolinium enhancement cardiovascular magnetic resonance predicts clinical worsening in patients with pulmonary hypertension. J Cardiovasc Magn Reson. 2012;14:11. [PubMed: 22296860]

23. Friedberg MK, Cho MY, Li J, Assad RS, Sun M, Rohailla S, Honjo O, Apitz C and Redington AN. Adverse biventricular remodeling in isolated right ventricular hypertension is mediated by increased transforming growth factor-beta1 signaling and is abrogated by angiotensin receptor blockade. American journal of respiratory cell and molecular biology. 2013;49:1019–28. [PubMed: 23841477]

24. Marsboom G, Wietholt C, Haney CR, Toth PT, Ryan JJ, Morrow E, Thenappan T, Bache-Wiig P, Piao L, Paul J, et al. Lung (1)(8)F-fluorodeoxyglucose positron emission tomography for diagnosis

and monitoring of pulmonary arterial hypertension. Am J Respir Crit Care Med. 2012;185:670–9. [PubMed: 22246173]

25. Zhang H, Wang D, Li M, Plecita-Hlavata L, D'Alessandro A, Tauber J, Riddle S, Kumar S, Flockton A, McKeon BA, et al. Metabolic and Proliferative State of Vascular Adventitial Fibroblasts in Pulmonary Hypertension Is Regulated Through a MicroRNA-124/PTBP1 (Polypyrimidine Tract Binding Protein 1)/Pyruvate Kinase Muscle Axis. Circulation. 2017;136:2468–2485. [PubMed: 28972001]

26. Li M, Riddle S, Zhang H, D'Alessandro A, Flockton A, Serkova NJ, Hansen KC, Moldvan R, McKeon BA, Frid M, et al. Metabolic Reprogramming Regulates the Proliferative and Inflammatory Phenotype of Adventitial Fibroblasts in Pulmonary Hypertension Through the Transcriptional Corepressor C-Terminal Binding Protein-1. Circulation. 2016;134:1105–1121. [PubMed: 27562971]

27. Plecita-Hlavata L, Tauber J, Li M, Zhang H, Flockton AR, Pullamsetti SS, Chelladurai P, D'Alessandro A, El Kasmi KC, Jezek P and Stenmark KR. Constitutive Reprogramming of Fibroblast Mitochondrial Metabolism in Pulmonary Hypertension. American journal of respiratory cell and molecular biology. 2016;55:47–57. [PubMed: 26699943]

28. Caruso P, Dunmore BJ, Schlosser K, Schoors S, Dos Santos C, Perez-Iratxeta C, Lavoie JR, Zhang H, Long L, Flockton AR, et al. Identification of MicroRNA-124 as a Major Regulator of Enhanced Endothelial Cell Glycolysis in Pulmonary Arterial Hypertension via PTBP1 (Polypyrimidine Tract Binding Protein) and Pyruvate Kinase M2. Circulation. 2017;136:2451–2467. [PubMed: 28971999]

29. Fijalkowska I, Xu W, Comhair SA, Janocha AJ, Mavrakis LA, Krishnamachary B, Zhen L, Mao T, Richter A, Erzurum SC and Tuder RM. Hypoxia inducible-factor1alpha regulates the metabolic shift of pulmonary hypertensive endothelial cells. The American journal of pathology. 2010;176:1130–8. [PubMed: 20110409]

30. Piao L, Fang YH, Cadete VJ, Wietholt C, Urboniene D, Toth PT, Marsboom G, Zhang HJ, Haber I, Rehman J, et al. The inhibition of pyruvate dehydrogenase kinase improves impaired cardiac function and electrical remodeling in two models of right ventricular hypertrophy: resuscitating the hibernating right ventricle. Journal of molecular medicine. 2010;88:47–60. [PubMed: 19949938]

31. Sutendra G, Dromparis P, Paulin R, Zervopoulos S, Haromy A, Nagendran J and Michelakis ED. A metabolic remodeling in right ventricular hypertrophy is associated with decreased angiogenesis and a transition from a compensated to a decompensated state in pulmonary hypertension. Journal of molecular medicine. 2013;91:1315–27. [PubMed: 23846254]

32. Paulin R, Sutendra G, Gurtu V, Dromparis P, Haromy A, Provencher S, Bonnet S and Michelakis ED. A miR-208-Mef2 axis drives the decompensation of right ventricular function in pulmonary hypertension. Circulation research. 2015;116:56–69. [PubMed: 25287062]

33. Piao L, Sidhu VK, Fang YH, Ryan JJ, Parikh KS, Hong Z, Toth PT, Morrow E, Kutty S, Lopaschuk GD and Archer SL. FOXO1-mediated upregulation of pyruvate dehydrogenase kinase-4 (PDK4) decreases glucose oxidation and impairs right ventricular function in pulmonary hypertension: therapeutic benefits of dichloroacetate. Journal of molecular medicine. 2013;91:333–46. [PubMed: 23247844]

34. Michelakis ED, Gurtu V, Webster L, Barnes G, Watson G, Howard L, Cupitt J, Paterson I, Thompson RB, Chow K, et al. Inhibition of pyruvate dehydrogenase kinase improves pulmonary arterial hypertension in genetically susceptible patients. Sci Transl Med. 2017;9.

35. Bonnet S, Michelakis ED, Porter CJ, Andrade-Navarro MA, Thebaud B, Bonnet S, Haromy A, Harry G, Moudgil R, McMurtry MS, et al. An abnormal mitochondrial-hypoxia inducible factor-1alpha-Kv channel pathway disrupts oxygen sensing and triggers pulmonary arterial hypertension in fawn hooded rats: similarities to human pulmonary arterial hypertension. Circulation. 2006;113:2630–41. [PubMed: 16735674]

36. Zhao L, Ashek A, Wang L, Fang W, Dabral S, Dubois O, Cupitt J, Pullamsetti SS, Cotroneo E, Jones H, et al. Heterogeneity in lung (18)FDG uptake in pulmonary arterial hypertension: potential of dynamic (18)FDG positron emission tomography with kinetic analysis as a bridging biomarker for pulmonary vascular remodeling targeted treatments. Circulation. 2013;128:1214–24. [PubMed: 23900048]

37. Manalo DJ, Rowan A, Lavoie T, Natarajan L, Kelly BD, Ye SQ, Garcia JG and Semenza GL. Transcriptional regulation of vascular endothelial cell responses to hypoxia by HIF-1. Blood. 2005;105:659–69. [PubMed: 15374877]

38. Archer SL, Marsboom G, Kim GH, Zhang HJ, Toth PT, Svensson EC, Dyck JR, Gomberg-Maitland M, Thebaud B, Husain AN, Cipriani N and Rehman J. Epigenetic attenuation of mitochondrial superoxide dismutase 2 in pulmonary arterial hypertension: a basis for excessive cell proliferation and a new therapeutic target. Circulation. 2010;121:2661–71. [PubMed: 20529999]

39. Xu W, Koeck T, Lara AR, Neumann D, DiFilippo FP, Koo M, Janocha AJ, Masri FA, Arroliga AC, Jennings C, et al. Alterations of cellular bioenergetics in pulmonary artery endothelial cells. Proceedings of the National Academy of Sciences of the United States of America. 2007;104:1342–7. [PubMed: 17227868]

40. McMurtry MS, Bonnet S, Wu X, Dyck JR, Haromy A, Hashimoto K and Michelakis ED. Dichloroacetate prevents and reverses pulmonary hypertension by inducing pulmonary artery smooth muscle cell apoptosis. Circulation research. 2004;95:830–40. [PubMed: 15375007]

41. Tian L, Potus F, Wu D, Dasgupta A, Chen KH, Mewburn J, Lima P and Archer SL. Increased Drp1-Mediated Mitochondrial Fission Promotes Proliferation and Collagen Production by Right Ventricular Fibroblasts in Experimental Pulmonary Arterial Hypertension. Front Physiol. 2018;9:828. [PubMed: 30042687]

42. Dweep H and Gretz N. miRWalk2.0: a comprehensive atlas of microRNA-target interactions. Nat Methods. 2015;12:697. [PubMed: 26226356]

43. Bonnet S, Boucherat O, Paulin R, Wu D, Hindmarch CCT, Archer SL, Song R, Moore JBt, Provencher S, Zhang L and Uchida S. Clinical value of non-coding RNAs in cardiovascular, pulmonary, and muscle diseases. Am J Physiol Cell Physiol. 2020;318:C1–C28. [PubMed: 31483703]

44. Chen KH, Dasgupta A, Lin J, Potus F, Bonnet S, Iremonger J, Fu J, Mewburn J, Wu D, Dunham-Snary K, et al. Epigenetic Dysregulation of the Dynamin-Related Protein 1 Binding Partners MiD49 and MiD51 Increases Mitotic Mitochondrial Fission and Promotes Pulmonary Arterial Hypertension: Mechanistic and Therapeutic Implications. Circulation. 2018;138:287–304. [PubMed: 29431643]

45. Marsboom G, Toth PT, Ryan JJ, Hong Z, Wu X, Fang YH, Thenappan T, Piao L, Zhang HJ, Pogoriler J, et al. Dynamin-related protein 1-mediated mitochondrial mitotic fission permits hyperproliferation of vascular smooth muscle cells and offers a novel therapeutic target in pulmonary hypertension. Circulation research. 2012;110:1484–97. [PubMed: 22511751]

46. Andersen S, Birkmose Axelsen J, Ringgaard S, Randel Nyengaard J, Holm Nielsen S, Genovese F, Asser Karsdal M, Adler Hyldebrandt J, Brandt Sorensen C, de Man FS, et al. Pressure overload induced right ventricular remodeling is not attenuated by the anti-fibrotic agent pirfenidone. Pulmonary circulation. 2019;9:2045894019848659. [PubMed: 30997866]

47. Sztrymf B, Souza R, Bertoletti L, Jais X, Sitbon O, Price LC, Simonneau G and Humbert M. Prognostic factors of acute heart failure in patients with pulmonary arterial hypertension. Eur Respir J. 2010;35:1286–93. [PubMed: 19897557]

48. Campo A, Mathai SC, Le Pavec J, Zaiman AL, Hummers LK, Boyce D, Housten T, Lechtzin N, Chami H, Girgis RE and Hassoun PM. Outcomes of hospitalisation for right heart failure in pulmonary arterial hypertension. Eur Respir J. 2011;38:359–67. [PubMed: 21310884]

49. Kim JW, Tchernyshyov I, Semenza GL and Dang CV. HIF-1-mediated expression of pyruvate dehydrogenase kinase: a metabolic switch required for cellular adaptation to hypoxia. Cell Metab. 2006;3:177–85. [PubMed: 16517405]

50. Kluza J, Corazao-Rozas P, Touil Y, Jendoubi M, Maire C, Guerreschi P, Jonneaux A, Ballot C, Balayssac S, Valable S, et al. Inactivation of the HIF-1alpha/PDK3 signaling axis drives melanoma toward mitochondrial oxidative metabolism and potentiates the therapeutic activity of pro-oxidants. Cancer Res. 2012;72:5035–47. [PubMed: 22865452]

51. Prigione A, Rohwer N, Hoffmann S, Mlody B, Drews K, Bukowiecki R, Blumlein K, Wanker EE, Ralser M, Cramer T and Adjaye J. HIF1alpha modulates cell fate reprogramming through early glycolytic shift and upregulation of PDK1–3 and PKM2. Stem Cells. 2014;32:364–76. [PubMed: 24123565]

52. Paulin R and Michelakis ED. The metabolic theory of pulmonary arterial hypertension. Circulation research. 2014;115:148–64. [PubMed: 24951764]

53. Archer SL, Weir EK and Wilkins MR. Basic science of pulmonary arterial hypertension for clinicians: new concepts and experimental therapies. Circulation. 2010;121:2045–66. [PubMed: 20458021]

54. Fang YH, Piao L, Hong Z, Toth PT, Marsboom G, Bache-Wiig P, Rehman J and Archer SL. Therapeutic inhibition of fatty acid oxidation in right ventricular hypertrophy: exploiting Randle's cycle. Journal of molecular medicine. 2012;90:31–43. [PubMed: 21874543]

55. Archer SL. Pyruvate Kinase and Warburg Metabolism in Pulmonary Arterial Hypertension: Uncoupled Glycolysis and the Cancer-Like Phenotype of Pulmonary Arterial Hypertension. Circulation. 2017;136:2486–2490. [PubMed: 29255124]

56. Bowker-Kinley MM, Davis WI, Wu P, Harris RA and Popov KM. Evidence for existence of tissue-specific regulation of the mammalian pyruvate dehydrogenase complex. The Biochemical journal. 1998;329 (Pt 1):191–6. [PubMed: 9405293]

57. Kaewpila S, Venkataraman S, Buettner GR and Oberley LW. Manganese superoxide dismutase modulates hypoxia-inducible factor-1 alpha induction via superoxide. Cancer Res. 2008;68:2781–8. [PubMed: 18413745]

58. Tian L, Neuber-Hess M, Mewburn J, Dasgupta A, Dunham-Snary K, Wu D, Chen KH, Hong Z, Sharp WW, Kutty S and Archer SL. Ischemia-induced Drp1 and Fis1-mediated mitochondrial fission and right ventricular dysfunction in pulmonary hypertension. Journal of molecular medicine. 2017;95:381–393. [PubMed: 28265681]

59. Hong Z, Chen KH, DasGupta A, Potus F, Dunham-Snary K, Bonnet S, Tian L, Fu J, Breuils-Bonnet S, Provencher S, et al. MicroRNA-138 and MicroRNA-25 Down-regulate Mitochondrial Calcium Uniporter, Causing the Pulmonary Arterial Hypertension Cancer Phenotype. Am J Respir Crit Care Med. 2017;195:515–529. [PubMed: 27648837]

60. Warburg O On the origin of cancer cells. Science. 1956;123:309–14. [PubMed: 13298683]

61. Zhou G, Dada LA, Wu M, Kelly A, Trejo H, Zhou Q, Varga J and Sznajder JI. Hypoxia-induced alveolar epithelial-mesenchymal transition requires mitochondrial ROS and hypoxia-inducible factor 1. Am J Physiol Lung Cell Mol Physiol. 2009;297:L1120–30. [PubMed: 19801454]

62. Higgins DF, Biju MP, Akai Y, Wutz A, Johnson RS and Haase VH. Hypoxic induction of Ctgf is directly mediated by Hif-1. Am J Physiol Renal Physiol. 2004;287:F1223–32. [PubMed: 15315937]

63. Semenza GL. Hypoxia-inducible factor 1 and cardiovascular disease. Annu Rev Physiol. 2014;76:39–56. [PubMed: 23988176]

64. Prins KW, Tian L, Wu D, Thenappan T, Metzger JM and Archer SL. Colchicine Depolymerizes Microtubules, Increases Junctophilin-2, and Improves Right Ventricular Function in Experimental Pulmonary Arterial Hypertension. Journal of the American Heart Association. 2017;6.

65. Lourenco AP, Roncon-Albuquerque R Jr.,, Bras-Silva C, Faria B, Wieland J, Henriques-Coelho T, Correia-Pinto J and Leite-Moreira AF. Myocardial dysfunction and neurohumoral activation without remodeling in left ventricle of monocrotaline-induced pulmonary hypertensive rats. American journal of physiology Heart and circulatory physiology. 2006;291:H1587–94. [PubMed: 16679394]

66. Crnkovic S, Egemnazarov B, Damico R, Marsh LM, Nagy BM, Douschan P, Atsina K, Kolb TM, Mathai SC, Hooper JE, Ghanim B, Klepetko W, Fruhwald F, Lassner D, Olschewski A, Olschewski H, Hassoun PM and Kwapiszewska G. Disconnect between Fibrotic Response and Right Ventricular Dysfunction. Am J Respir Crit Care Med. 2019;199:1550–1560. [PubMed: 30557518]

67. Bogaard HJ and Voelkel NF. Is Myocardial Fibrosis Impairing Right Heart Function? Am J Respir Crit Care Med. 2019;199:1458–1459. [PubMed: 30608865]

68. Bruns DR, Tatman PD, Kalkur RS, Brown RD, Stenmark KR, Buttrick PM and Walker LA. The right ventricular fibroblast secretome drives cardiomyocyte dedifferentiation. PloS one. 2019;14:e0220573. [PubMed: 31374110]

69. Jiang B, Deng Y, Suen C, Taha M, Chaudhary KR, Courtman DW and Stewart DJ. Marked Strain-Specific Differences in the SU5416 Rat Model of Severe Pulmonary Arterial Hypertension. American journal of respiratory cell and molecular biology. 2016;54:461–8. [PubMed: 26291195]

70. Rafikov R, Sun X, Rafikova O, Meadows ML, Desai AA, Khalpey Z, Yuan JX, Fineman JR and Black SM. Complex I dysfunction underlies the glycolytic switch in pulmonary hypertensive smooth muscle cells. Redox biology. 2015;6:278–86. [PubMed: 26298201]

71. Urboniene D, Haber I, Fang YH, Thenappan T and Archer SL. Validation of high-resolution echocardiography and magnetic resonance imaging vs. high-fidelity catheterization in experimental pulmonary hypertension. Am J Physiol Lung Cell Mol Physiol. 2010;299:L401–12. [PubMed: 20581101]

72. Andersen MJ, Hwang SJ, Kane GC, Melenovsky V, Olson TP, Fetterly K and Borlaug BA. Enhanced pulmonary vasodilator reserve and abnormal right ventricular: pulmonary artery coupling in heart failure with preserved ejection fraction. Circ Heart Fail. 2015;8:542–50. [PubMed: 25857307]

73. Melenovsky V, Hwang SJ, Lin G, Redfield MM and Borlaug BA. Right heart dysfunction in heart failure with preserved ejection fraction. Eur Heart J. 2014;35:3452–62. [PubMed: 24875795]

74. Guazzi M, Bandera F, Pelissero G, Castelvecchio S, Menicanti L, Ghio S, Temporelli PL and Arena R. Tricuspid annular plane systolic excursion and pulmonary arterial systolic pressure relationship in heart failure: an index of right ventricular contractile function and prognosis. Am J Physiol Heart Circ Physiol. 2013;305:H1373–81. [PubMed: 23997100]

75. Guazzi M, Naeije R, Arena R, Corrà U, Ghio S, Forfia P, Rossi A, Cahalin LP, Bandera F and Temporelli P. Echocardiography of right ventriculoarterial coupling combined with cardiopulmonary exercise testing to predict outcome in heart failure. Chest. 2015;148:226–34. [PubMed: 25633590]

76. Prins KW, Weir EK, Archer SL, Markowitz J, Rose L, Pritzker M, Madlon-Kay R and Thenappan T. Pulmonary pulse wave transit time is associated with right ventricular-pulmonary artery coupling in pulmonary arterial hypertension. Pulm Circ. 2016;6:576–585. [PubMed: 28090301]

77. Agocha AE and Eghbali-Webb M. A simple method for preparation of cultured cardiac fibroblasts from adult human ventricular tissue. Mol Cell Biochem. 1997;172:195–8. [PubMed: 9278245]

78. Neuss M, Regitz-Zagrosek V, Hildebrandt A and Fleck E. Isolation and characterisation of human cardiac fibroblasts from explanted adult hearts. Cell Tissue Res. 1996;286:145–53. [PubMed: 8781221]

79. Lund J, Ouwens DM, Wettergreen M, Bakke SS, Thoresen GH and Aas V. Increased Glycolysis and Higher Lactate Production in Hyperglycemic Myotubes. Cells. 2019;8.

80. Rehman J, Zhang HJ, Toth PT, Zhang Y, Marsboom G, Hong Z, Salgia R, Husain AN, Wietholt C and Archer SL. Inhibition of mitochondrial fission prevents cell cycle progresssion in lung cancer. FASEB journal. 2012;26:2175–86. [PubMed: 22321727]

NOVELTY AND SIGNIFICANCE

What Is Known?

- Right ventricular (RV) failure in pulmonary arterial hypertension (PAH) is associated with

- increased RV fibrosis.

- RV fibroblasts (RVfib) in PAH are hyperproliferative and profibrotic.

- The Warburg effect (uncoupled glycolysis) occurs in the RV in PAH

What New Information Does This Article Contribute?

- A Warburg mitochondrial metabolic phenotype occurs in RVfib in PAH and causes a proliferative,

- profibrotic, phenotype.

- This pathologic RVfib phenotype, which persists despite passage of cells in culture, is triggered by epigenetic inhibition of superoxide dismutase 2 (SOD2) by DNA methyltransferase 1 (DNMT1).

- The resulting reduced redox environment causes normoxic activation in hypoxia-inducible factor 1-alpha (HIF-1α) leading to increased expression/ activity of pyruvate dehydrogenase kinase (PDK) isoforms 1 and 3 and production of fibrogenic cytokines like transforming growth factor beta 1 (TGF–β1) and connective tissue growth factor (CTGF).

The fundamental cause of RV fibrosis is unknown. While resident RVfib are responsible for fibrosis, these cells are understudied. This study examined the genesis and consequences of abnormal mitochondrial metabolism in RVfib derived from rats with MCT-induced PAH. We demonstrate that DNMT1-mediated DNA methylation is increased in RVfib driving redox changes that activate HIF-1α and cause a proliferative, fibrogenic RVfib phenotype that persists despite passage of cells in culture. HIF-1α upregulates PDK expression and increases fibrogenic cytokines, like TGF-β1 and CTGF. Decompensated human PAH RVs also show increased RV fibrosis and have increased PDK1 expression in RVfib. PDK inhibition reverses the mitochondrial-metabolic phenotype and decreases fibroblast proliferation and collagen production in vitro. Consistent with this, dichloroacetate improves pulmonary hemodynamics, reduces RV fibrosis and improves RV function in vivo in a preclinical model of PAH. This work establishes the epigenetic basis for RV fibrosis and demonstrates that it is therapeutically tractable. We can now add RVfib to the cells in PAH that have a shared Warburg metabolic basis for dysfunction.
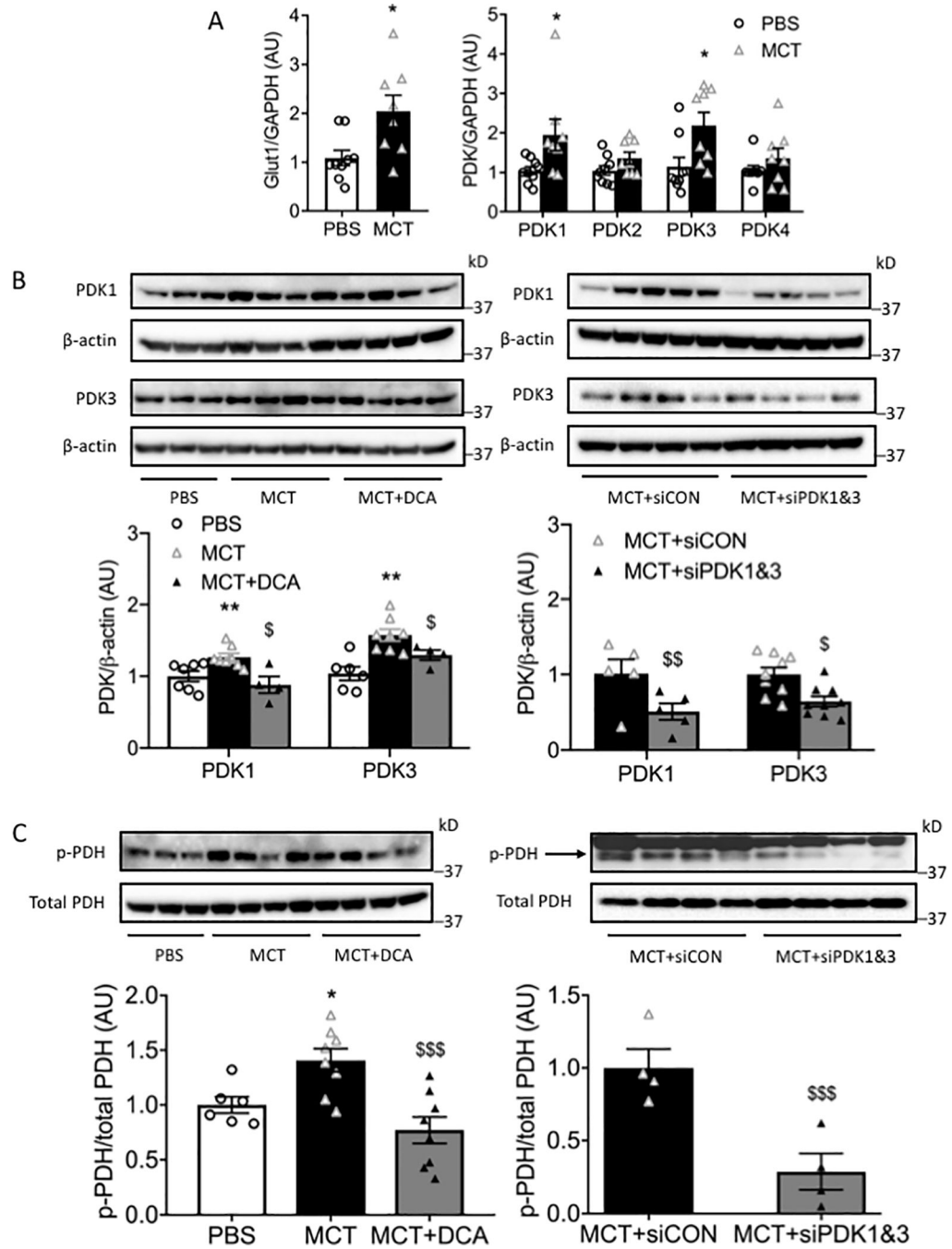
Figure 1. PDK1 and PDK3 are the predominant isoforms upregulated in MCT-RVfib.
Compared to control, monocrotaline (MCT)-derived RV fibroblasts (MCT-RVfib) display upregulation in glucose transporter 1 (Glut1), pyruvate dehydrogenase kinase (PDK) isoform 1 & 3, and phosphorylated pyruvate dehydrogenase (p-PDH). Both sodium dichloroacetate (DCA) and small interfering RNA (siRNA) targeting PDK isoforms 1 & 3 (siPDK1&3) treatments reduce PDK1, PDK3 and p-PDH in MCT-RVfib. (A) mRNA expression of Glut1 (P=0.027 by student's *t*-test; n=9 and n=8 for PBS and MCT groups, respectively) and 4 isoforms of PDK (P=0.015, 0.12, 0.01 and 0.49 by student's *t*-test for comparison in PDK1,

PDK2, PDK3 and PDK4, respectively; n=9 for PDK1, PDK2 and PDK3 of PBS groups and n=8 for the other groups). (B) Immunoblotting of PDK1 and PDK3 with treatment of DCA or siPDK1&3 (The sample sizes for PBS, MCT and MCT+DCA groups are: 7, 8 and 4 respectively for measurement of PDK1, and 6, 8 and 4 respectively for measurement of PDK3. The sample sizes for MCT+siCON (control siRNA) and MCT+siPDK1&3 are: both 5 for measurement of PDK1 and both 9 for measurement of PDK3. P=0.0068 and 0.014 by student's t-test for MCT vs. PBS and MCT+DCA vs. MCT respectively in PDK1; P=0.001 and 0.049 by student's t-test for MCT vs. PBS and MCT+DCA vs. MCT respectively in PDK3; P=0.0093 and 0.042 by paired t-test for MCT+siPDK1&3 vs. MCT+siCON in PDK1 and PDK3, respectively). (C) Immunoblotting of p-PDH with DCA or siPDK1&3 treatment (n=6, 8 and 8 for PBS, MCT and MCT+DCA groups, respectively. n=4 for both MCT +siCON and MCT+siPDK1&3 groups. P=0.013 and 0.0003 by student's and paired t-test respectively for MCT vs. PBS and MCT+DCA vs. MCT, respectively. P=0.001 by paired t-test for MCT+siPDK1&3 vs. MCT+siCON). siCON, control siRNA. *, P<0.05 and **, P<0.01 versus PBS group; $, P<0.05, $ $, P<0.01 and $ $ $, P<0.001 versus the corresponding vehicle control group (MCT or MCT+siCON group). Immunoblotting images were taken with Chemidoc MP Imaging System and analyzed with ImageJ.
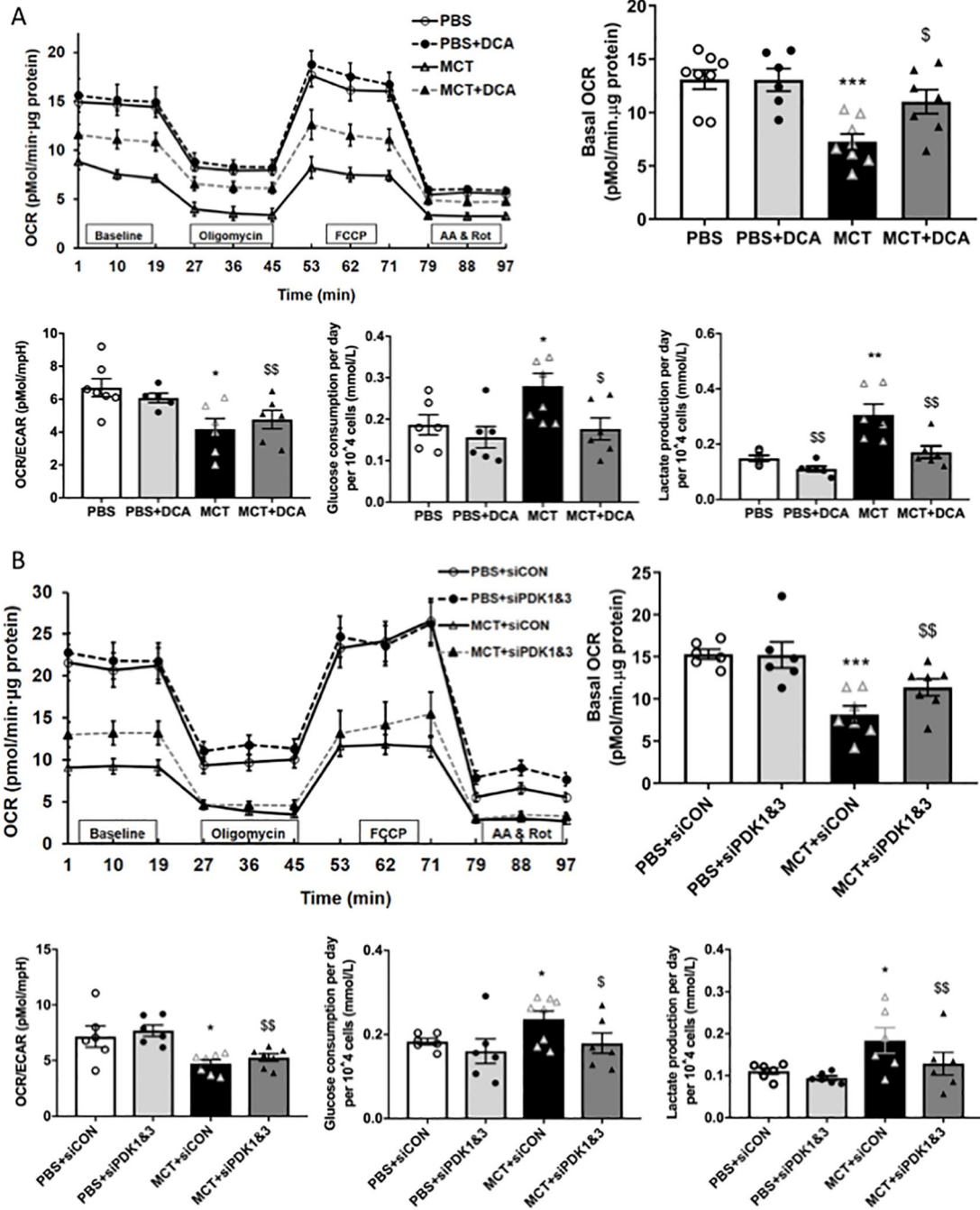
Figure 2. Warburg Metabolism in MCT-RVfib is mediated by PDK1&3

Monocrotaline (MCT)-derived RV fibroblasts (MCT-RVfib) display lower oxygen consumption rate (OCR), higher glucose consumption and lactate production, and a lower ratio of OCR to extracellular acidification rate (ECAR) (OCR/ECAR), compared to control. Both sodium dichloroacetate (DCA) and small interfering RNA (siRNA) targeting pyruvate dehydrogenase kinase (PDK) isoforms 1&3 (siPDK1&3) treatments increase OCR and OCR/ECAR, and reduce glucose consumption and lactate production in MCT-RVfib. Note that the glucose consumption and lactate production are lower in the cells with DCA

treatment than that with siPDK1&3 treatment. This likely reflects that DCA was replaced daily as DCA-treated cells received new culture medium daily whereas the culture medium for siRNA-treated cells was not changed during the course of the protocol. Representative OCR measurement via Seahorse XF^{e}24 Extracellular Flux Analyzer and summary of basal OCR, OCR/ECAR, glucose consumption and lactate production in cell culture medium with treatment of (A) DCA and (B) siPDK1&3. (A) The sample sizes for PBS, PBS+DCA, MCT, MCT+DCA groups are: 8, 6, 8 and 7 in basal OCR measurement respectively, 7, 5, 6 and 6 in OCR/ECAR measurement respectively, 6, 6, 8 and 6 in the measurement of glucose consumption respectively, and 6 for all the groups in the measurement of lactate production. P values by student's or paired t-test for PBS+DCA vs. PBS, MCT vs. PBS and MCT+DCA vs. MCT are 0.98, 0.0002 and 0.013 respectively in basal OCR, 0.40, 0.012 and 0.0076 respectively in OCR/ECAR, 0.18, 0.043 and 0.031 respectively in glucose consumption, and 0.0015, 0.0028 and 0.0057 respectively in lactate production. (B) The sample sizes for PBS +siCON, PBS+siPDK1&3, MCT+siCON, MCT+siPDK1&3 groups are: 6, 6, 7 and 7 in both basal OCR and OCR/ECAR measurements respectively, 6, 6, 8, 6 for in the measurement of glucose consumption, and 6 for all the groups in the measurement of lactate production. P values by student's or paired t-test for PBS+siPDK1&3 vs. PBS+siCON, MCT+siCON vs. PBS+siCON and MCT+siPDK1&3 are: 0.94, 0.0001 and 0.016 respectively in basal OCR, 0.44, 0.025 and 0.0094 respectively in OCR/ECAR, 0.42, 0.041 and 0.037 respectively in glucose consumption, and 0.11, 0.043 and 0.0065 respectively in lactate production. FCCP, carbonyl cyanide 4-(trifluoromethoxy)phenylhydrazone; AA, antimycin A; Rot, rotenone; siCON, control siRNA. *, P<0.05, **, P<0.01 and ***, P<0.001 versus PBS or PBS+siCON group; $, P<0.05, $ $, P<0.01 and $ $ $, P<0.001 versus the corresponding vehicle control group (MCT or MCT+siCON group).
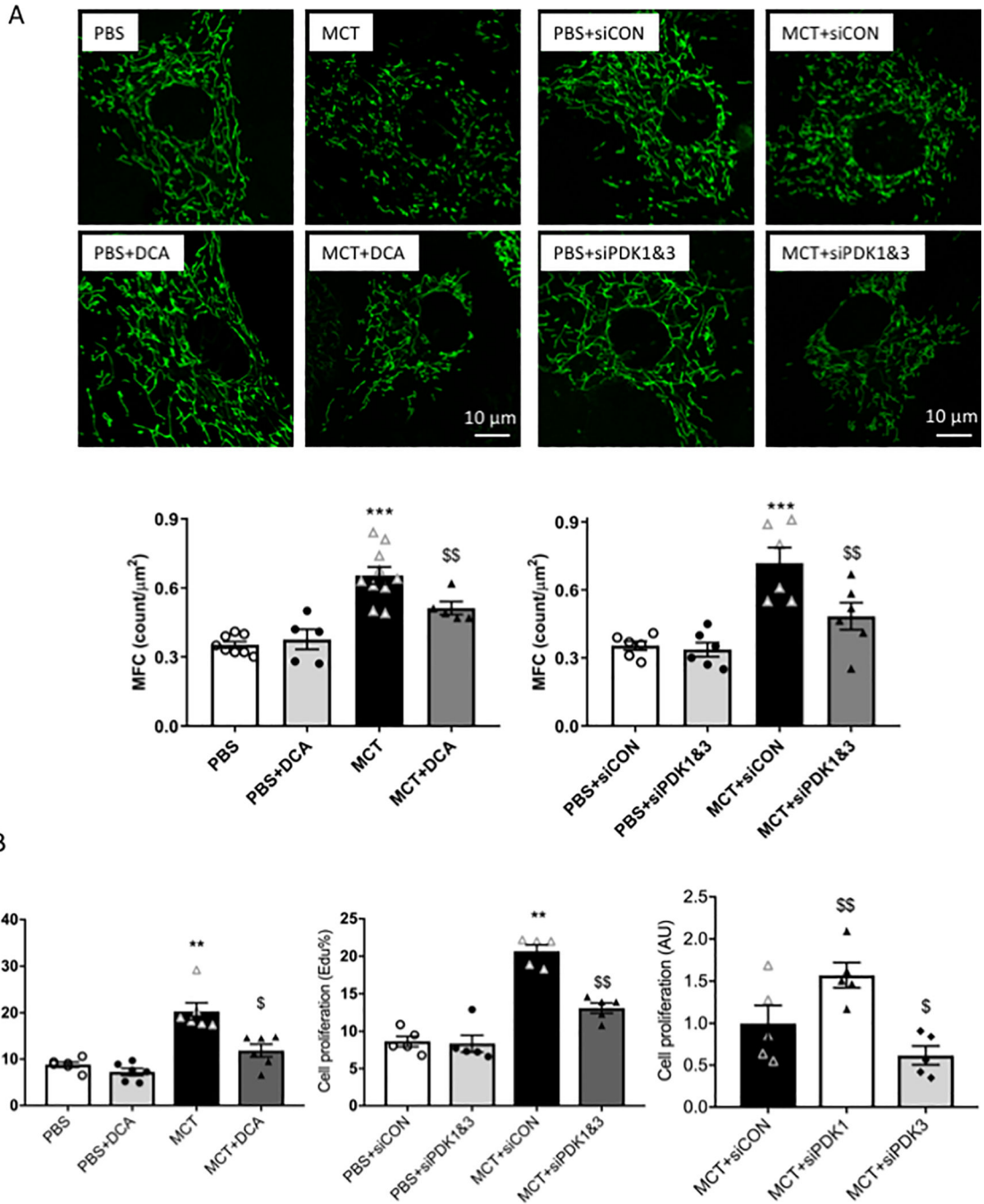
Figure 3. Increased mitochondrial fission and proliferation in MCT-RVfib are mediated by PDK1&3

Monocrotaline (MCT)-derived RV fibroblasts (MCT-RVfib) display excess mitochondrial fission and increased proliferation rate compared to control. Both sodium dichloroacetate (DCA) and small interfering RNA (siRNA) targeting pyruvate dehydrogenase kinase (PDK) isoforms 1 & 3 (siPDK1&3) treatments inhibit mitochondrial fission and decrease proliferation rate in MCT-RVfib, and only siPDK3 (not siPDK1) reduced proliferation rate in MCT-RVfib. (A) Representative mitochondrial network stained with MitoTracker™ Green FM in RVfib with DCA or siPDK1&3 treatment and the summary of mitochondrial

fragmentation count (MFC) (n=8, 5, 10 and 5 for PBS, PBS+DCA, MCT and MCT+DCA groups, respectively. P=0.56, 0.0000035 and 0.0093 by student's t-test for PBS+DCA vs. PBS, MCT vs. PBS and MCT+DCA vs. MCT, respectively. n=6 for PBS+siCON, PBS +siPDK1&3, MCT+siCON and MCT+siPDK1&3 groups. P=0.43 and 0.0025 by paired t-test for PBS+siPDK1&3 vs. PBS+siCON and MCT+siPDK1&3 vs. MCT+siCON, respectively. P=0.0005 by student's t-test for MCT+siCON vs. PBS+ siCON). (B) Summary of proliferation rates (n=6 for PBS, PBS+DCA, MCT and MCT+DCA groups and n=5 for the other groups. P=0.07 and 0.03 by paired t-test for PBS+DCA vs. PBS and MCT+DCA vs. MCT, respectively. P=0.0022 by student's t-test for MCT vs. PBS. P=0.81 and 0.0056 by paired t-test for PBS+siPDK1&3 vs. PBS+siCON and MCT+siPDK1&3 vs. MCT+siCON, respectively. P=0.0079 by student's t-test for MCT+siCON vs. PBS+ siCON. P= 0.006 and 0.049 by ANOVA followed by Tukey's post hoc test for MCT+siPDK1 vs. MCT+siCON and MCT+siPDK3 vs. MCT+siCON, respectively). siCON, control siRNA. **, P<0.01, and ***, P<0.001 versus PBS or PBS+siCON group; $, P<0.05 and $ $, P<0.01 versus the corresponding vehicle control group (MCT or MCT+siCON group). Immunofluorescent images were taken with a Leica SP8 confocal, laser-scanning microscope and analyzed with ImageJ.
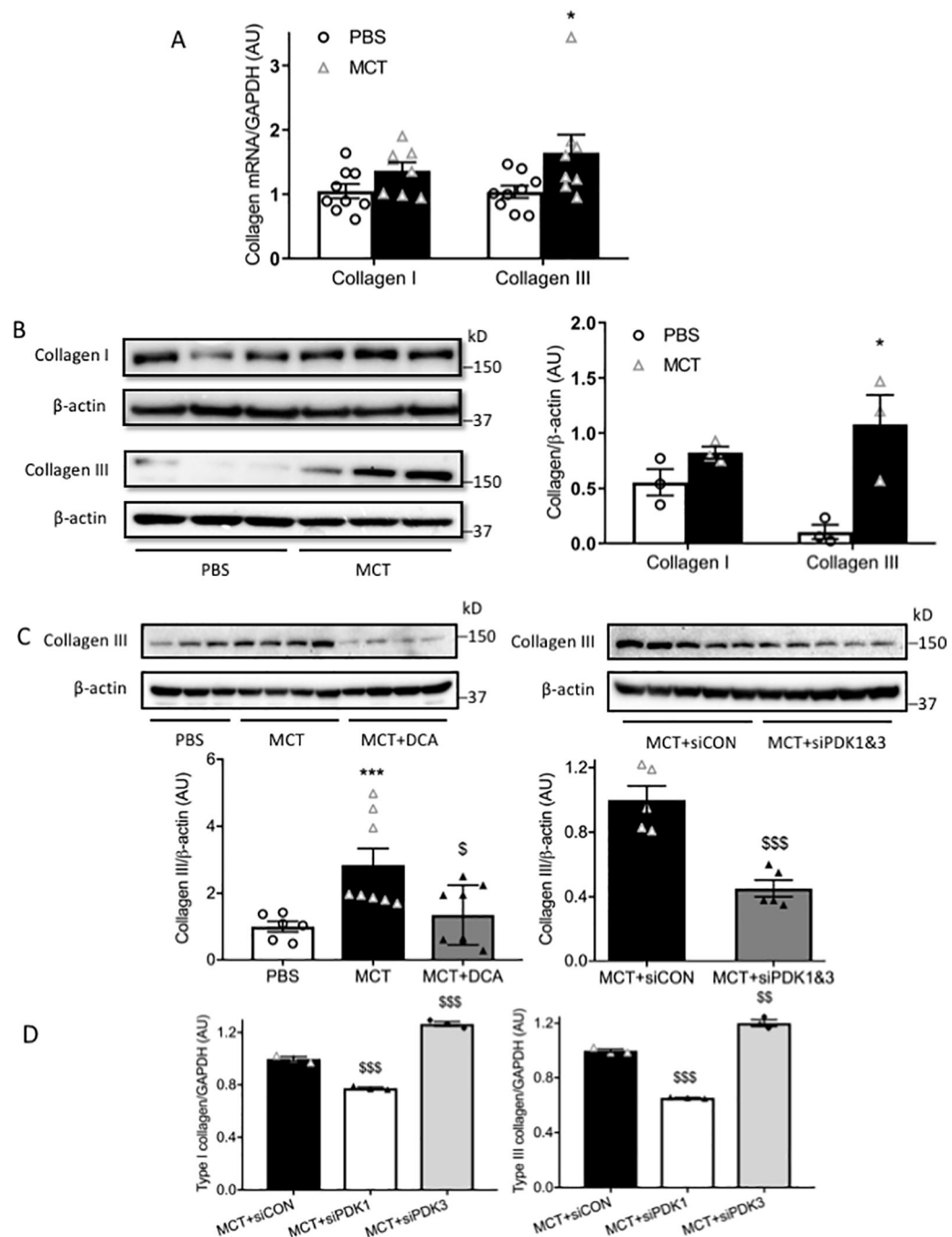
Figure 4. Increased production of type III collagen in MCT-RVfib is mediated by PDK1&3

Monocrotaline (MCT)-derived RV fibroblasts (MCT-RVfib) have greater collagen production in type III compared to control. Both sodium dichloroacetate (DCA) and small interfering RNA (siRNA) targeting pyruvate dehydrogenase kinase (PDK) isoforms 1 & 3 (siPDK1&3) treatments reduce type III collagen production in MCT-RVfib, and only siPDK1 (not siPDK3) reduced type I and III collagen production. (A) mRNA expression of type I and III collagen (n=9 and 8 for PBS and MCT groups, respectively. P=0.072 and 0.045 by student's *t*-test for MCT vs. PBS in type I collagen and type III collagen,

respectively); (B) Immunoblotting of type I and III collagen (n=3 per group. P=0.11 and 0.024 by student's *t*-test for MCT vs. PBS in collagen I and collagen III, respectively); (C) Immunoblotting of type III collagen in RVfib treated with DCA or siPDK1&3 (n=6, 8, 8, 5 and 5 for PBS, MCT, MCT+DCA, MCT+siCON and MCT+siPDK1&3 groups, respectively. P=0.0007 and 0.016 by student's or paired *t*-test for MCT vs. PBS and MCt+DCA vs. MCT respectively. P=0.0002 by paired *t*-test for MCT+siPDK1&3 vs. MCT+siCON); (D) Effects of siPDK1 and siPDK3 individually on type I and III collagen mRNA in a MCT-RVfib cell line with triplicate measurement using qRT-PCR analysis (P=0.0009 and 0.0005 by ANOVA followed by Tukey's post hoc test for MCT+siPDK1 vs. MCT+siCON and MCT+siPDK3 vs. MCT+siCON respectively in type I collagen; P=0.0002 and 0.018 with ANOVA followed by Tukey's post hoc test for MCT+siPDK1 vs. MCT+siCON and MCT+siPDK3 vs. MCT+siCON respectively in type III collagen;). siCON, control siRNA. *, P<0.05, **, P<0.01, and ***, P<0.001versus PBS group; $, P<0.05, $ $, P<0.01, and $ $ $, P<0.001 versus the corresponding vehicle control group (MCT or MCT+siCON group). Immunoblotting images were taken with Chemidoc MP Imaging System and analyzed with ImageJ.
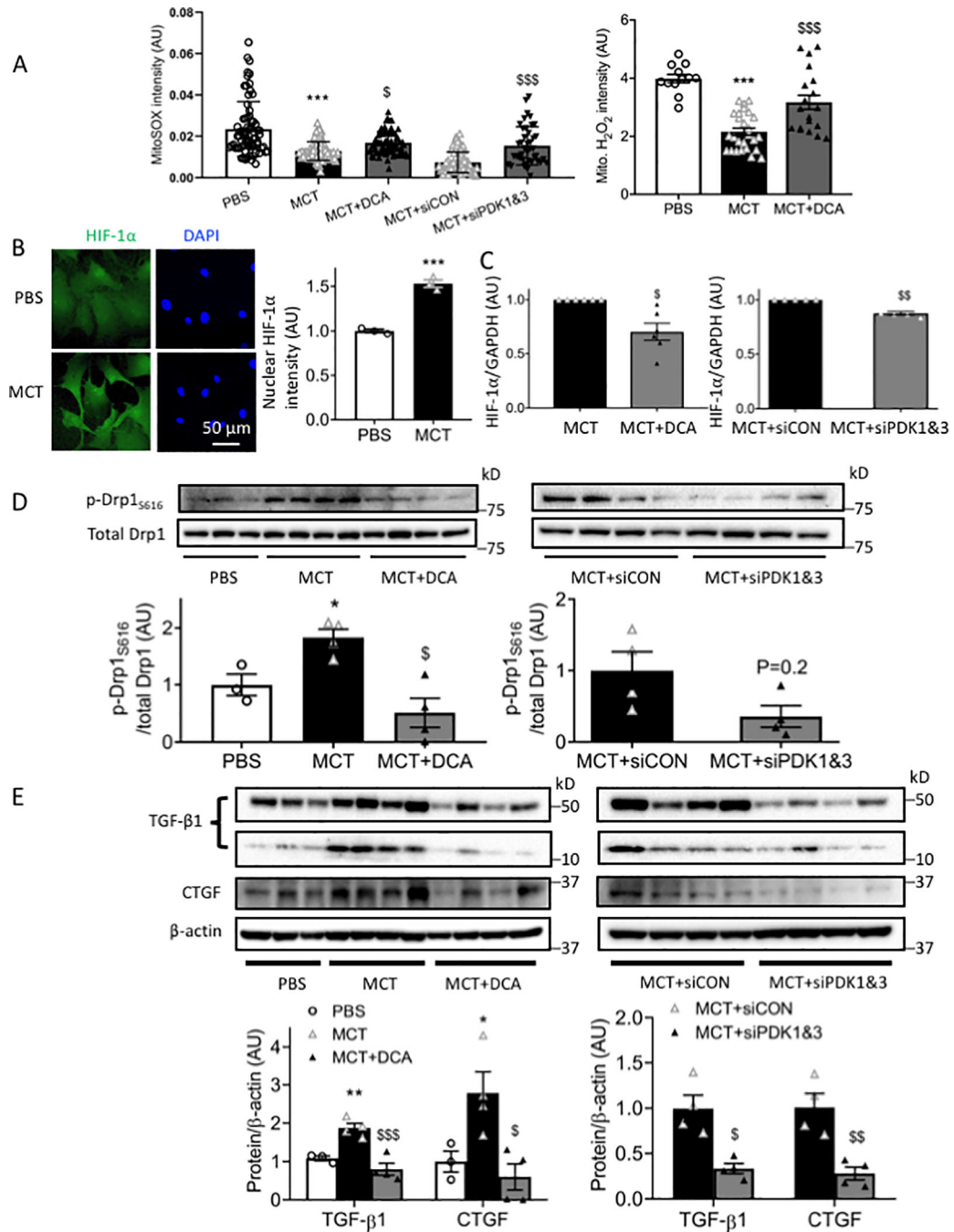
Figure 5. Impaired mitochondrial redox signaling, Drp1 activation and production of fibrogenic cytokines in MCT-RVfib are mediated by PDK1&3.
Compared to control, monocrotaline (MCT)-derived RV fibroblasts (MCT-RVfib) display decrease in the production of mitochondrial (Mito.) superoxide (MitoSOX) and H_2O_2 and increases in the intensity of nuclear hypoxia-inducible factor 1-alpha (HIF-1α), phosphorylated dynamin-related protein 1 at Serine 616 (p-Drp1$_{S616}$), transforming growth factor beta-1 (TGF-β1), and connective tissue growth factor (CTGF). All these changes are reversed by both sodium dichloroacetate (DCA) and small interfering RNA (siRNA) targeting pyruvate dehydrogenase kinase (PDK) isoforms 1 & 3 (siPDK1&3) treatments. (A)

Summary of fluorescence intensity of MitoSOX (n=72, 75, 75, 80 and 42 cells from PBS, MCT, MCT+DCA, MCT+siCON and MCT+siPDK1&3 groups respectively were analyzed. P=8.8×10^{-10}, 0.021 and 0.0000033 by ANOVA followed by Tukey's post hoc test for MCT vs. PBS, MCT+DCA vs. MCT and MCT+siDPK1&3 vs. MCT+siCON, respectively) and mitochondrial H_2O_2 (n=12, 26 and 19 cells from PBS, MCT and MCT+DCA groups respectively were analyzed. P=4.4×10^{-8} and 0.0002 by ANOVA followed by Tukey's post hoc test for MCT vs. PBS and MCT+DCA vs. MCT, respectively). (B) Representative immunofluorescent images of HIF-1α in RVfib and summary of the fluorescence intensity in the nuclei (more than 95 cells from 3 cell lines per group were analyzed; P=0.0003 by student's *t*-test). (C) mRNA expression of HIF-1α in MCT-RVfib treated with DCA or siPDK1&3 (n=6 for both MCT and MCT+DCA groups. n=5 for both MCT+siCON and MCT+siPDK1&3 groups. P=0.025 and 0.0019 by paired *t*-test for MCT+DCA vs. MCT and MCT+siPDK1&3 vs. MCT+siCON, respectively). (D) Immunoblotting of p-Drp1$_{S616}$ (n=3, 4, 4, 4, and 4 for PBS, MCT, MCT+DCA, MCT+siCON and MCT+siPDK1&3 groups, respectively. P=0.017 and 0.047 by student's or paired *t*-test for MCT vs. PBS and MCT +DCA vs. MCT, respectively. P=0.2 by paired *t*-test for MCT+siPDK1&3 vs. MCT +siCON). (E) Immunoblotting of TGF-β1 and CTGF (n=3, 4, 4, 4 and 4 for PBS, MCT, MCT+DCA, MCT+siCON and MCT+siPDK1&3 groups, respectively. P=0.0033 and 0.0004 by student's or paired *t*-test for MCT vs. PBS and MCT+DCA vs. MCT respectively in TGF-β1. P=0.049 and 0.011 by student's or paired *t*-test for MCT vs. PBS and MCT +DCA vs. MCT respectively in CTGF. P=0.029 and 0.0033 by paired *t*-test for MCT +siPDK1&3 vs. MCT+siCON in TGF-β1 and CTGF, respectively). siCON, control siRNA. *, P<0.05, **, P<0.01 and ***, P<0.001 versus PBS group; $, P<0.05, $ $, P<0.01 and $ $ $, P<0.001 versus the corresponding vehicle control group (MCT or MCT+siCON group). Immunoblotting images were taken with Chemidoc MP Imaging System and analyzed with ImageJ. Immunofluorescent images were taken with a Leica SP8 confocal, laser-scanning microscope and analyzed with ImageJ.
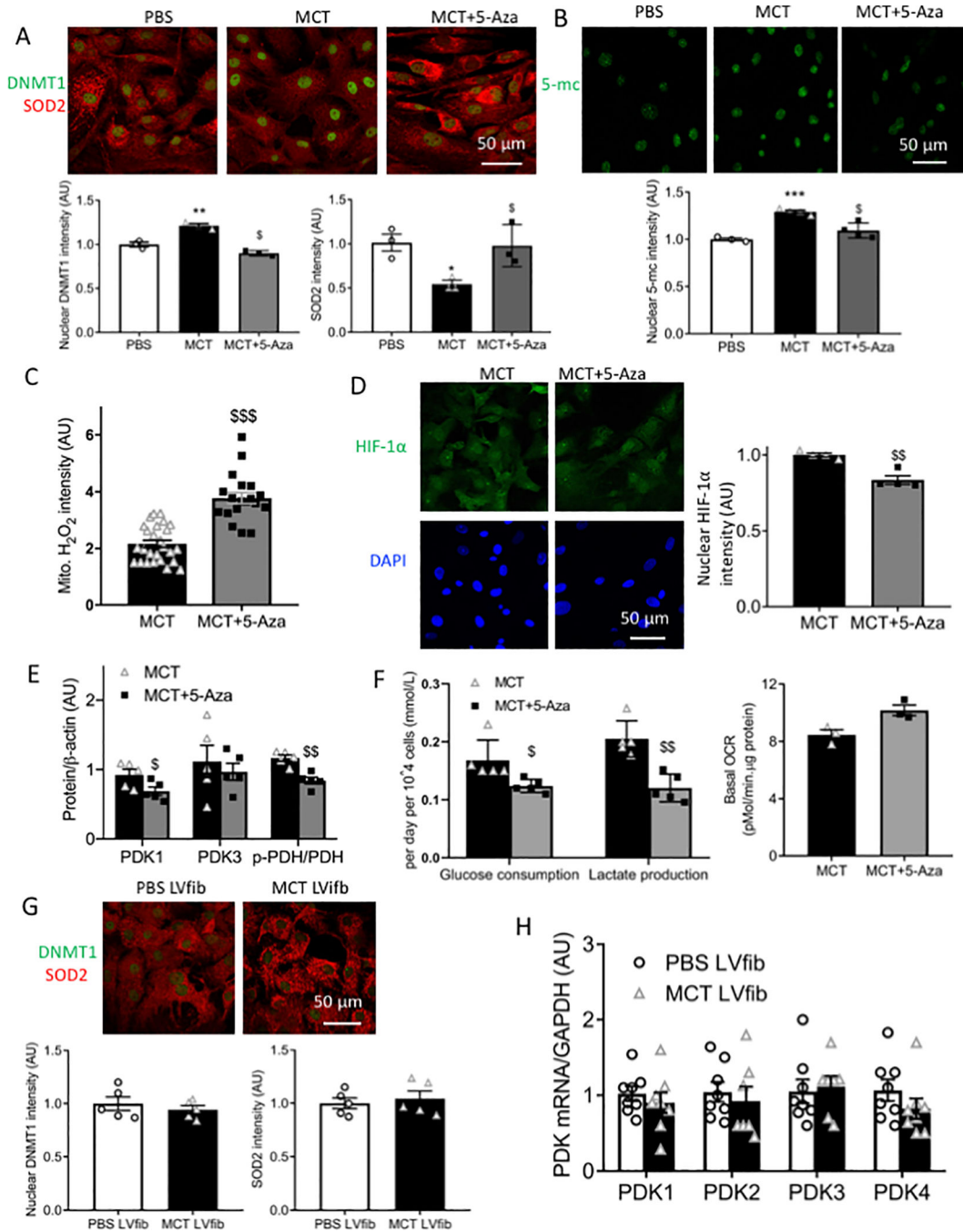
Figure 6. Increased DNA methyltransferase activity underlies the chamber-specific changes in mitochondrial redox signaling, HIF-1α activation and PDK expression in MCT-RVfib

Compared to control, monocrotaline (MCT)-derived RV fibroblasts (MCT-RVfib) display increases in the expression of DNA methyltransferase 1 (DNMT1) and 5-methylcytosin (5-mc) and a decrease in the expression of superoxide dismutase 2 (SOD2). Treatment with 5-Azacytidine (5-Aza) in MCT-RVfib restores these changes, increases the production of mitochondrial (Mito.) H_2O_2, reduces nuclear hypoxia-inducible factor 1-alpha (HIF-1α), and restores the mitochondrial metabolism. Whereas in left ventricular fibroblasts (LVfib) there was no difference in the expression of DNMT1, SOD2 or pyruvate dehydrogenase

kinase (PDK) between MCT and control groups. (A) Representative immunofluorescent images of DNMT1 and SOD2 and summary of the fluorescence intensity (more than 90 cells from 3 cell lines per group were analyzed; P=0.0039 by student's t-test for MCT vs. PBS in DNMT1 and P=0.017 by paired t-test for MCT+5-Aza vs. MCT in DNMT1. P=0.012 by student's t-test for MCT vs. PBS in SOD2 and P=0.043 by paired t-test for MCT +5-Aza vs. MCT in SOD2). (B) Representative immunofluorescent images of 5-mc in RVfib and summary of the fluorescence intensity in the nuclei (more than 120 cells from 3 cell lines in PBS group and 4 cell lines in MCT and MCT+5-Aza groups were analyzed. P=0.000052 by student's t-test for MCT vs. PBS and P=0.029 by paired t-test for MCT+5-Aza vs. MCT). (C) Summary of the fluorescence intensity of mitochondrial H_2O_2 (n=19 cells per group were analyzed. P=6.3×10^{-8} by student's t-test). (D) Representative immunofluorescent images of HIF-1α in MCT-RVfib treated with 5-Azacytidine and summary of the fluorescence intensity in the nuclei (more than 80 cells from 4 cell lines per group were analyzed. P=0.038 by paired t-test). (E) Summary of immunoblotting data on the expression of PDK isoform 1 (PDK1), PDK3, the phosphorylated pyruvate dehydrogenase (p-PDH)/total PDH ratio (n=5 per group. P=0.019, 0.67 and 0.0062 by paired t-test in PDK1, PDK3 and p-PDH, respectively). (F) Summary of glucose consumption (n=5 per group. P=0.026), lactate production (n=5 per group. P=0.0026) and oxygen consumption rate (OCR) (n=3 per group. P=0.0776). Paired t-test was used. (G) Representative immunofluorescent images of DNMT1 and SOD2 in LVfib and summary of the fluorescence intensity (n = 5 per group. P=0.47 and 0.62 by student's t-test for MCT vs. PBS LVfib in DNMT1 and SOD2, respectively). (H) mRNA expression of 4 PDK isoforms in LVfib (P=0.59, 0.33, 0.64 and 0.17 by student's t-test for PDK1, PDK2, PDK3 and PDK4, respectively. n=7 for MCT PDK2 and PDK3 groups, and n=8 for the other groups). *, P<0.05, **, P<0.01 and ***, P<0.001 versus PBS group; $, P<0.05, $ $, P<0.01 and $ $ $, P<0.001 versus the MCT group. Immunofluorescent images were taken with a Leica SP8 confocal, laser-scanning microscope and analyzed with ImageJ.
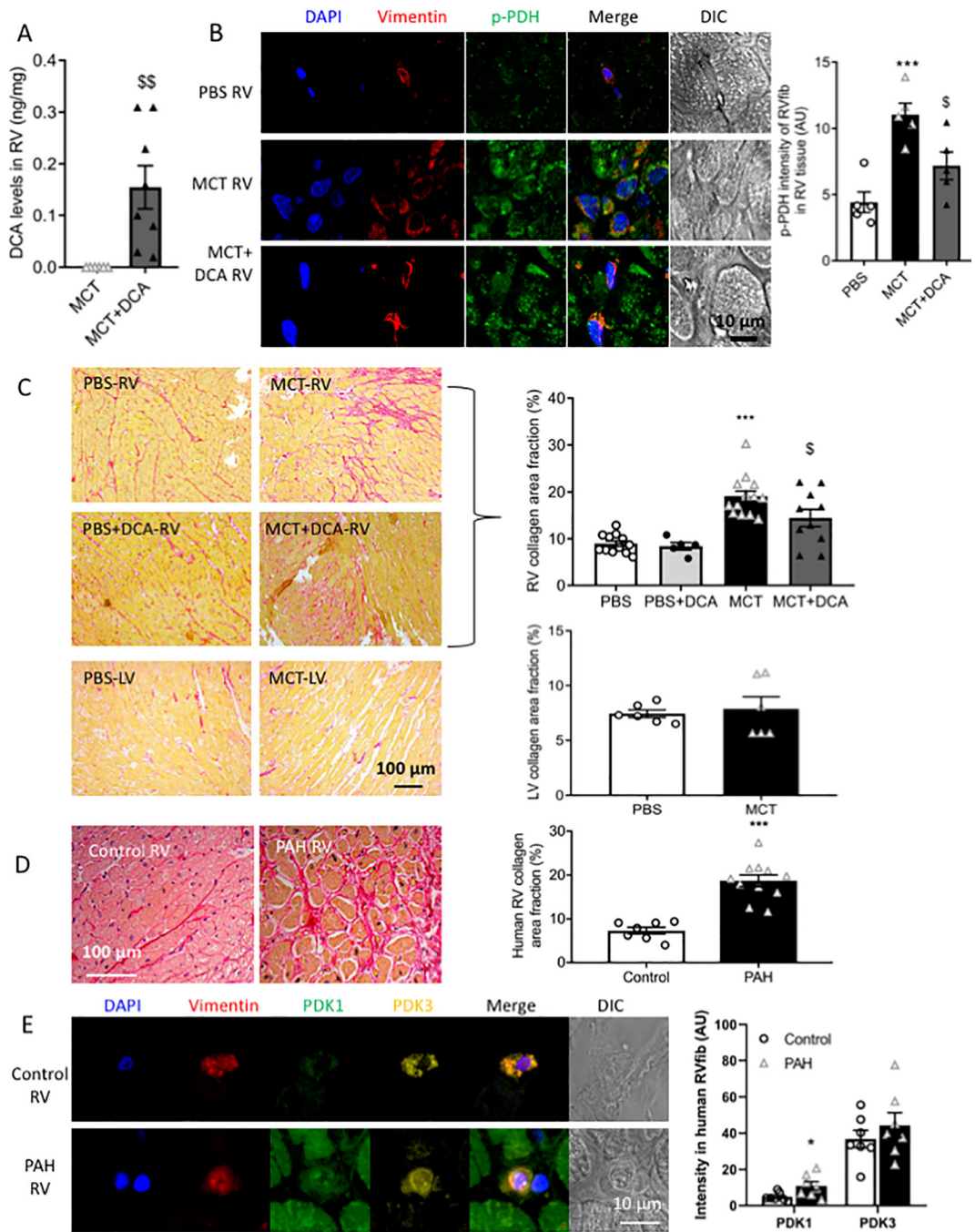
Figure 7. DCA is effective in reducing phospho-PDH expression *in vivo* and PDK1 is the predominant isoform in the fibrotic RVs of patients with PAH and RVF

Monocrotaline (MCT) rats developed greater right ventricular (RV) fibrosis and had higher phosphorylated pyruvate dehydrogenase (p-PDH) levels in RV fibroblasts (RVfib) than control, and treatment with sodium dichloroacetate (DCA) reduced RV fibrosis and p-PDH levels in RVfib in MCT rats. In contrast, left ventricles (LVs) from MCT rats did not develop greater fibrosis than control. RV from pulmonary arterial hypertension (PAH) patients displayed greater fibrosis and had higher expression of pyruvate dehydrogenase kinase isoform 1 (PDK1) in fibroblasts than control. (A) Summary of DCA levels measured using

mass spectrometry in RVs from MCT (n=6) and DCA-treated MCT (n=8) rats (P=0.0076 by student's *t*-test). (B) Representative immunofluorescent images of p-PDH in RV tissues and summary of fluorescence intensity of vimentin-positive cells, i.e., RVfib (n=5 per group. P=0.0007 and 0.029 by ANOVA followed by Tukey's post hoc test for MCT vs. PBS and MCT+DCA vs. MCT, respectively). (C) Representative picrosirius red-stained images of RVs or LVs from rats and summary of collagen area fraction (n=12, 5, 14 and 10 RVs from PBS, PBS+DCA, MCT, MCT+DCA groups, respectively. n=6 LVs from PBS and MCT groups. P=0.99, 0.0000010 and 0.04 by ANOVA followed by Tukey's post hoc test for PBS +DCA vs. PBS, MCT vs. PBS and MCT+DCA vs. MCT in RV collagen area fraction, respectively. P=0.71 by student's *t*-test for MCT vs. PBS in LV collagen area fraction). (D) Representative picrosirius red-stained images of RVs from patients and summary of collagen area fraction (n=7 and 11 for control and PAH patients, respectively. P=0.000052 by student's *t*-test for PAH vs. control). (E) Representative immunofluorescent images of PDK1 and PDK3 in vimentin-positive cells (RVfib) (n=7 per group. P=0.049 and 0.39 by student's *t*-test in PDK1 and PDK3, respectively). DIC, differential interference contrast. *, P<0.05 and ***, P<0.001 versus control (or PBS) group; \$, P<0.05 and \$ \$, P<0.01 versus the MCT group. Immunofluorescent images were taken with a Leica SP8 confocal, laser-scanning microscope and analyzed with ImageJ. Histology images were taken with a Leica digital color camera attached to a Leica DM4 microscope and analyzed with a Leica software (LAS V4.7).
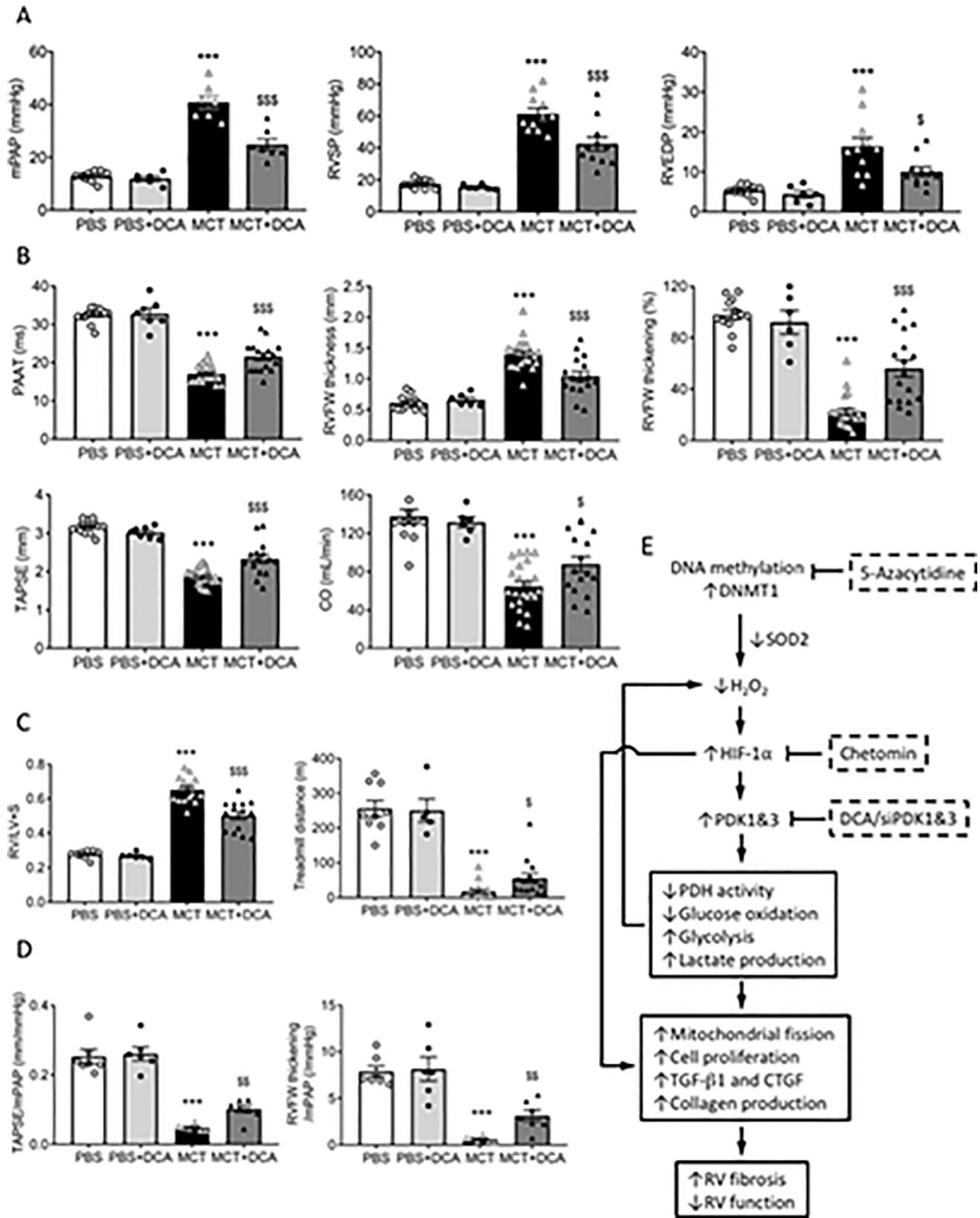
Figure 8. The PDK inhibitor dichloroacetate is effective in reversing MCT RVF *in vivo*
Monocrotaline (MCT) rats developed right ventricular (RV) hypertrophy, dysfunction and pulmonary hypertension, and treatment with sodium dichloroacetate (DCA) improved RV function in MCT rats. (A) Summary of mean pulmonary artery pressure (mPAP) and RV systolic and end-diastolic pressures (RVSP and RVEDP, respectively) (The sample sizes for PBS, PBS+DCA, MCT and MCT+DCA groups are: 9, 6, 7, and 7 respectively in mPAP measurement, and 10, 6, 11 and 11 respectively in both RVSP and RVEDP measurements. P-values for PBS+DCA vs. PBS, MCT vs. PBS and MCT+DCA vs. MCT are: 0.98,

7.9×10^{-9} and 3.6×10^{-6} respectively in mPAP, 0.98, 7.1×10^{-11} and 0.0006 respectively in RVSP, and 0.98, 0.000027 and 0.015 respectively in RVEDP). (B) Summary of hemodynamic measurements via echocardiography on pulmonary artery acceleration time (PAAT), RV free wall (RVFW) thickness, RVFW thickening, tricuspid annular plane systolic excursion (TAPSE) and cardiac output (CO) (The sample sizes for PBS, PBS+DCA, MCT and MCT+DCA groups are: 13, 7, 23 and 16 respectively in PAAT measurement, 14, 6, 23 and 17 respectively in RVFW thickness measurement, 13, 6, 23 and 17 respectively in RVFW thickening measurement, 14, 7, 23 add 15 respectively in TAPSE measurement, and 12, 6, 23 and 16 respectively in CO measurement. P-values for PBS+DCA vs. PBS, MCT vs. PBS and MCT+DCA vs. MCT are 0.63, 3.6×10^{-12} and 0.000018 respectively in TAPSE, 0.96, 7.4×10^{-12} and 0.000054 respectively in RVFW thickness, and 0.93, 1.6×10^{-14} and 0.00031 respectively in RVFW thickening). (C) Summary of Fulton index [ratio of RV weight to left ventricle plus septum weight (LV+S), i.e., RV/LV+S] and treadmill distance (The sample sizes for PBS, PBS+DCA, MCT and MCT+DCA groups are: 9, 6, 16 and 15 respectively in RV/LV+S measurement and 9, 5, 13 and 15 respectively in treadmill distance measurement. P-values for PBS+DCA vs. PBS, MCT vs. PBS and MCT+DCA vs. MCT are: 0.99, 8.2×10^{-13} and 0.0000018 respectively in RV/LV+S, and 0.97, 8.3×10^{-10} and 0.039 respectively in CO). (D) RV-PA coupling quantified by TAPSE/mPAP and RVFW thickening/mPAP (The sample sizes for PBS, PBS+DCA, MCT and MCT+DCA groups are 7, 6, 6 and 7 respectively. P-values for PBS+DCA vs. PBS, MCT vs. PBS and MCT+DCA vs. MCT are: 0.95, 9.8×10^{-9} and 0.07 respectively in TAPSE/mPAP, and 0.99, 3.6×10^{-6} and 0.1 respectively in RVFW thickening/mPAP. P=0.001 and 0.0027 by student's *t*-test for MCT+DCA vs. MCT in TAPSE/mPAP and RVFW thickening/mPAP, respectively). (E) Proposed mechanistic pathway for the contribution of DNA methylation, pyruvate dehydrogenase kinase (PDK) and the associated Warburg metabolic phenotype to RV fibroblasts function in pulmonary arterial hypertension (PAH). DNMT1, DNA methyltransferase 1; SOD2, superoxide dismutase 2; HIF-1α, hypoxia-inducible factor 1-alpha; PDH, pyruvate dehydrogenase; siPDK1&3, small interfering RNA targeting PDK isoforms 1&3, TGF-β1, transforming growth factor beta-1; CTGF, connective tissue growth factor. The Tukey's post hoc test after ANOVA was performed. ***, P<0.001 versus PBS group; $, P<0.05, $ $, P<0.01 and $ $ $, P<0.001 versus the MCT group.